AD-A139 463 GROWTH RATES OF PARAMETRIC INSTABILITIES DRIVEN BY TWO PUMPS(U) CALIFORNIA UNIV LOS ANGELES CENTER FOR PLASMA PHYSICS AND FUS.. J L MILOVICH ET AL. JAN 84 PPG-763 1/1

UNCLASSIFIED N00014-75-C-0476 F/G 12/1 NL

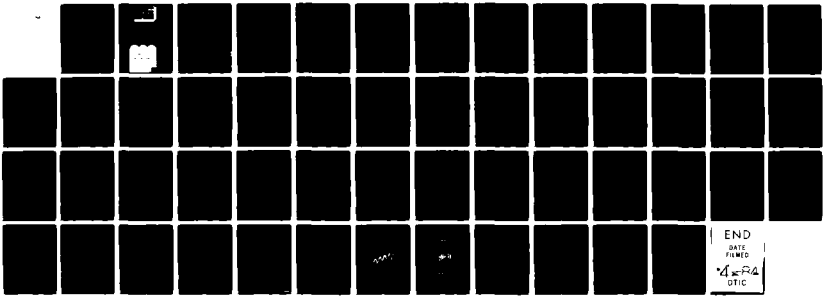

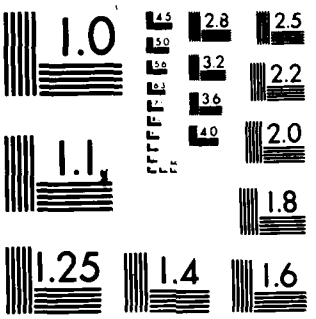

GROWTH RATES OF PARAMETRIC INSTABILITIES DRIVEN BY TWO PUMPS

J. L. Milovich, B. D. Fried & C. J. Morales

PPG-763 January, 1984

Contract N00014-75-C-0476

CENTER FOR PLASMA PHYSICS AND FUSION ENGINEERING

UNIVERSITY OF CALIFORNIA LOS ANGELES

GROWTH RATES OF PARAMETRIC INSTABILITIES DRIVEN BY TWO PUMPS

J. L. Milovich, B. D. Fried & G. J. Morales

PPG-763 January, 1984

Contract N00014-75-C-0476

Department of Physics

University of California

Los Angeles, California 90024

Abstract

The parametric instability growth rate of ion acoustic and Langmuir waves, driven unstable by two uniform pumps near the Bohm-Gross frequency, is calculated as a function of pump amplitudes and frequencies. Two instability mechanisms can be identified: one corresponds to the usual, single pump parametric instabilities (decay and oscillating two stream) while the other is similar to that found in the Mathieu equation. The interaction between these two mechanisms results in a non-monotonic dependence of the growth rate on the pump amplitudes and frequencies: both cancellation and enhancement are obtained for various values of the parameters. An analytic study of the relevant dispersion relation using Hill's method is complemented by numerical studies in both the frequency and time domains.

I. INTRODUCTION

The growth rates of Langmuir and ion acoustic waves driven unstable by a high frequency uniform electric field $E_o(t) = E_1\cos\omega_1 t + E_2\cos\omega_2 t$ in a uniform unmagnetized plasma are calculated for "pump" frequencies ω_1 and ω_2 close to the Bohm-Gross frequency $\omega_k = (\omega_p^2 + 3T_e k^2/m)^{1/2}$, with the difference frequency $\Delta = \omega_1 - \omega_2$ being of order of the ion acoustic frequency $\Omega_k = kc_s$. While earlier work on this problem[1] considered the threshold for instability, i.e. the minimum value of $(E_1^2 + E_2^2)$ required to amplify a noise signal, we examine here the growth rate as a function of ω_1, ω_2, E_1 and E_2. Experimental observations on both experimental and ionospheric plasmas[2] have shown a complicated dependence of the wave amplitudes on pump frequencies. Although most steady-state experiments sample the nonlinearly saturated state of the instability, it is important to determine the properties of the early linear growth stage. The present work addresses this question and, in addition to providing the necessary conceptual framework for a future nonlinear saturation theory, predicts various nontrivial features which may be useful in understanding the experimental observations. Since most experiments operate well above the threshold levels, the damping of both Langmuir and ion-acoustic waves is neglected here; it then suffices to use the warm fluid theory rather than a kinetic theory model. The calculations can be extended to include damping terms but at the expense of introducing more parameters.

The characteristics of the usual single pump parametric excitation are well known. When the frequency matching condition $\omega_1 - \omega_k \simeq \Omega_k$, is satisfied there is a "decay instability", consisting of the decay of the pump wave at ω_1 into a Langmuir wave and an ion acoustic wave, both having wavenumber k. For any finite pump amplitude E_1 there is a range of ω_1 around $\omega_k + \Omega_k$ for which

the growth rate γ of the daughter waves is positive. Equivalently, for given ω_1 in that range, there is a threshold for E_1. Of course, when the frequency matching condition $\omega_1 = \omega_k + \Omega_k$ is satisfied exactly, the threshold drops to zero, when damping is neglected. When $\omega_1 \simeq \omega_k$, the so-called oscillating two-stream instability (OTSI) occurs, but here we shall discuss primarily the decay instability. All of these properties are immediate consequences of the fourth order differential equation which governs the time evolution of the spatial Fourier transform of the ion density $n_i(k, t)$. Since the coefficients of this equation are constants, its Laplace transform yields a simple dispersion equation, a quadratic in ω^2, whose solution gives the results stated previously.

With two pumps, the coefficients in the differential equation for n_i are not constant. Instead, they become periodic functions of t, with frequency $\Delta = \omega_1 - \omega_2$, resulting in a differential equation which resembles the well-known Mathieu equation, albeit of higher order. Physically, this Mathieu-like character arises from the ponderomotive force at the beat frequency Δ driving the ion acoustic waves. As might be expected, the solutions of this equation have properties analogous to those of the Mathieu equation.[3,4] Since the Laplace transform of this equation leads to an infinite set of coupled equations for the quantities $n_i(k, \omega \pm \ell\Delta)$, where ℓ is an integer, the dispersion relation takes the form of the vanishing of an infinite determinant, an equation which we solve for ω using Hill's method.[4]

The behavior of the resulting solutions can be described in terms of two separate instability mechanisms, one similar to the usual single pump parametric instability, the other analogous to that found in the Mathieu equation. Specifically, if ω_1 is near $\omega_k + \Omega_k$, if E_1 exceeds the single pump threshold E_s and if E_2 is of order E_1, we recover the usual decay instability, except for certain values of ω_2, where the growth rate γ vanishes or is slightly

enhanced. This is illustrated in Fig. 4 where the real and imaginary parts of ω for the growing wave are plotted as a function of ω_2 for fixed ω_1 and $E_1 = E_2$. In the figures, and in subsequent sections, we use the dimensionless quantities $\nu_\alpha = (\omega_\alpha - \omega_k)/\Omega_k$ and $g_\alpha = (eE_\alpha/T_e)(kk_D)^{-1/2}(M/16m)^{1/4}$ to characterize the pump frequencies and amplitudes. Fig. 4 illustrates some general features of the equal pump amplitude case with $E_1 = E_2 = E > E_s$. Although $\gamma \equiv \text{Im}\ \omega$ is equal to the single pump growth rate for most values of ω_2, it vanishes when $\nu_1 + \nu_2 = 0$ or $\nu_1 \pm \nu_2 = 2$ and it is enhanced slightly when $\nu_2 \simeq \nu_1 - 2/N$, where N is an integer, or when $\nu_2 \simeq 0$ (corresponding to the OTSI driven by the second pump). As we explain in more detail in Sec. IV, these results are representative of cases where the parametric decay instability tends to dominate the behavior but is modified by the Mathieu-like effects. (Further details concerning the results shown in Fig. 4 and in the other figures mentioned in this introductory section are given in Sec. IV.).

If ω_1 is near, but not exactly equal to $\omega_k + \Omega_k$ ($\nu_1 \simeq 1$) and E_1 is <u>below</u> the single pump threshold E_s corresponding to this value of ω_1, then only the Mathieu-like effects can produce instability, as illustrated in Fig. 5a, 5b, and 5c where $E = E_1 = E_2$ is successively increased, but remains below E_s. In Fig. 5d, where E exceeds E_s, one sees a combination of the two effects: the single pump decay mechanism dominates for ν_2 far from -1, while the Mathieu-like effects give enhanced growth near $\nu_2 = -1$ and zero growth for finite intervals of ν_2 above and below -1.

For unequal amplitudes, there is a complicated interplay between the Mathieu and decay mechanisms, the resulting behavior depending on the ratio E_2/E_1 and also the ratio E_1/E_s. If $E_1 < E_s$, the decay instability does not occur (unless $\nu_2 \simeq 1$) but the Mathieu instability appears, as illustrated in

Fig. 6a , the growth rate at first increasing as E_2 increases (Fig. 6b), and eventually decreasing (Fig. 6c). If E_1 is well above E_s, the second pump may simply modify the decay instability growth rate, as shown in Fig. 7a (details in Sec. IV) for $E_2 = E_1/2$, or it may, for larger E_2, actually suppress the growth rate entirely over a finite interval of ν_2 between the Mathieu and decay instability regions as in Fig. 7b.

If, instead of fixing ω_1 and varying ω_2 we keep ω_2 constant and vary ω_1, we observe a similar interaction of the two instability mechanisms as shown in Fig. 8. In general a mixture of the two mechanisms is most likely to occur when $\nu_1 \simeq 1$, maximizing the growth rate of the decay instability and, simultaneously $\nu_2 \simeq -1$ so that $\nu_1 - \nu_2 = \nu \simeq 2$ which corresponds to the strongest Mathieu-like instability. Most of our attention has been focused on this "mixed regime".

Since the parameter space (E_1, E_2, ω_1, ω_2) is four dimensional, surveying it is greatly facilitated by having an approximate solution of the dispersion equation. Judicious truncation of the infinite determinant yields a simple approximate dispersion equation (a biquadratic in ω) which gives close agreement with the exact results and also provides a simple means of understanding the propeties of the solution of the exact dispersion relation displayed in Figs. 5 through 8. In addition, this approximate dispersion relation can be used to determine the boundaries of the stable and unstable regions in the (E_1, E_2, ω_1, ω_2) space as illustrated in Fig. 3 for two-dimensional cross sections (E_2 vs. ν_2 for fixed E_1, ν_1; E_1 vs. ν_1 for fixed E_2, ν_2; E_2 vs. ν_1 for fixed E_1 and ν_2). Although this approximation can be strictly justified only when $\nu_1 \simeq -\nu_2 \simeq 1$, it proves to be valid, in fact, over a fairly broad range of parameter space, as illustrated in Fig. 9

As an alternative to the Laplace transform approach, we have also solved the differential equations in the time domain, using numerical integration, a procedure which avoids the various approximations used in solving the dispersion relation. Taking the Fourier transform of the solutions for $n_i(t)$ and $n_e(t)$ then gives directly the "line shapes" $n_i(\omega)$ and $n_e(\omega)$ which would be observed experimentally if the nonlinear saturation mechanism were independent of frequency. Although these quantities can also be calculated from the solutions of the Laplace transformed problem, that approach would give spectral peaks corresponding to all roots of the dispersion equation, growing, decaying, or stable, whereas in the time domain calculation (and in the experimental situation) the growing waves dominate. The time domain solutions also show clearly the modulational effects which result from the occurrence of two unstable roots of the dispersion equation.

The theoretical model used is presented in Sec. II, together with a derivation of the differential equation for $n_i(k, t)$ and a discussion of its similarity to the Mathieu equation. An exact solution of the frequency domain equations is given in Sec. III, where we also show that a judicious truncation of the infinite determinant leads to simple expressions for the frequencies and growth rates and for the boundaries of the stable and unstable regions in parameter space. The results of these numerical calculations and a discussion of the various features are presented in Sec. IV. Section V gives the solutions in the time domain for both growing and stable waves. Conclusions are presented in Sec. VI.

II. MODEL EQUATIONS AND DISPERSION RELATION

We consider a uniform, unmagnetized ion-electron plasma with a uniform "pump" electric field:

$$\underline{E}_o(t) = \underline{E}_1 \cos\omega_1 t + \underline{E}_2 \cos\omega_2 t \tag{1}$$

Pump depletion is neglected, so $\underline{E}_1$ and $\underline{E}_2$ are constant; $\underline{E}_1$ and $\underline{E}_2$ are assumed parallel; and the pump frequencies $\omega_j (j = 1, 2)$ are near the electron plasma frequency ω_p. Since we are interested in growth rates well above threshold, wave damping is neglected.

The fluid equations, for each species, $\alpha = e,i$,

$$\frac{\partial n_\alpha}{\partial t} + \nabla \cdot (n_\alpha \underline{v}_\alpha) = 0 \tag{2}$$

$$\frac{\partial \underline{v}_\alpha}{\partial t} + \underline{v}_\alpha \cdot \nabla \underline{v}_\alpha + \nabla p_\alpha / n_\alpha m_\alpha = q_\alpha \underline{E}/m_\alpha \tag{3}$$

are linearized about the oscillating motion due to $\underline{E}_o$

$$n_\alpha = n_o + n_{1\alpha}, \quad p_\alpha = p_{o\alpha} + p_{1\alpha}, \quad \underline{v}_\alpha = \underline{v}_{o\alpha} + \underline{v}_{1\alpha}, \quad \dot{\underline{v}}_{o\alpha} = q_\alpha \underline{E}_o / m_\alpha$$

This gives

$$\ddot{n}_{1\alpha} + 2(\underline{v}_{o\alpha} \cdot \nabla)\dot{n}_{1\alpha} + (\dot{\underline{v}}_{o\alpha} \cdot \nabla) n_{1\alpha} = \nabla^2 p_{1\alpha}/m_\alpha - (q_\alpha/m_\alpha) n_{o\alpha} \nabla \cdot (\underline{E} - \underline{E}_o) \tag{4}$$

if terms of order $v_{o\alpha}^2$ are neglected.

Using Poisson's equation; neglecting the zeroth order ion velocity (v_{oi}) since the ions do not respond to the high frequency field; setting $T_i = 0$ (i.e., taking the limit of large T_e/T_i); Fourier analyzing in space; and sep-

arating the electron density into high frequency (ω of order ω_p) and low frequency parts, $n_e = n_{eh} + n_{e\ell}$, we obtain

$$\ddot{n}_{eh} + \omega_k^2 n_{eh} = -ik\,(\dot{v}_o\, n_{e\ell}) \tag{5}$$

$$\omega_{pe}^2\,(n_{e\ell} - n_i) + k^2 T_e\, n_{e\ell}/m = ik\,(\dot{v}_o\, n_{eh})_\ell \tag{6}$$

$$\ddot{n}_i + \omega_{pi}^2\, n_i = \omega_{pi}^2\, n_{e\ell} \tag{7}$$

Here we have used $p_e = \sigma n_e T$ with $\sigma = 3$ for the high frequency and $\sigma = 1$ for the low frequency equation. Also, we set $m_e = m$, $m_i = M$, $\omega_k^2 = \omega_{pe}^2 + 3k^2 T_e/m$ and neglect terms of order m/M. Inserting (6) into (7) and approximating $\omega_{pi}^2\,[1 - \omega_{pe}^2/(\omega_{pe}^2 + k^2 T_e/M)] \simeq k^2 T_e/M = k^2\, c_s^2 \equiv \Omega_k^2$ we get

$$\ddot{n}_i + \Omega_k^2\, n_i = -(ike/M)(E_o n_{eh})_\ell \tag{8}$$

$$\ddot{n}_{eh} + \omega_k^2\, n_{eh} = (ike/m)(E_o n_i) \tag{9}$$

Note that the right hand side of (8) corresponds to the usual ponderomotive force. Finally, a modulational representation

$$n_{eh} = f_+(t)\,\exp(-i\omega_k t) + f_-(t)\,\exp(i\omega_k t) \tag{10}$$

where $f_\pm$ are slowly varying functions, $|\dot{f}_\pm/f_\pm| \ll \omega_k$, gives the equations:

$$\frac{\partial^2 n_i}{\partial \tau^2} + n_i = -\,(i\chi/2)[f_-(\tau)\Lambda(\tau) + f_+(\tau)\Lambda^*(\tau)] \tag{11}$$

$$\frac{\partial f_+}{\partial \tau} = -\,(\chi M/16m)^{1/2}\, n_i \Lambda \tag{12}$$

$$\frac{\partial f_-}{\partial \tau} = (\chi M/16m)^{1/2}\, n_i \Lambda^* \tag{13}$$

where

$$\Lambda = \sum_{j=1}^{2} \lambda_j \exp(-i\nu_j\tau), \qquad \lambda_j = (ekE_j/m\omega_p^2),$$

$$\nu_j = (\omega_j-\omega_k)/\Omega_k, \qquad \chi = (k_D/k)^2, \qquad \text{and} \qquad \tau = \Omega_k t.$$

The remainder of the paper is concerned with the properties of the solutions of (11) through (13). Of course, these equations are only valid for small λ_j since we have dropped terms of order v_o^2.

Before discussing the solution of (11) through (13), we note that solving (12) and (13) for $f_\pm$ and substituting the result into the ponderomotive force expression on the right side of (10) gives terms of the general form $\Lambda\,\Lambda^*\,n_i$. (The actual analysis, given later in this section, actually involves differentiating (10) to obtain a sixth order equation for n_i; the approximate discussion in this paragraph is only meant to illuminate the physics involved.) If there is only a single pump, $\Lambda\,\Lambda^*$ is constant so the equation for n_i has constant coefficients; the only effect is to change the eigenfrequency from $\omega = 1$ to a new value which, for pump amplitudes above the decay or OTSI thresholds, becomes complex. However, with two pumps, $\Lambda\,\Lambda^*$ contains also oscillating terms of frequency $\nu = \nu_1 - \nu_2$ and it is this oscillating ponderomotive force term in the ion density equation of motion which is responsible for the new effects arising with two pumps.

A direct method of solving these equations is to use the Laplace transform

$$n_i(\omega) = \int_o^\infty d\tau\; n_i(\tau)\exp(i\omega\tau)$$

(where ω is measured in units of Ω_k) which leads to the set of coupled equations

$$Y_-(\omega)n_i(\omega-\nu) + X(\omega)n_i(\omega) + Y_+(\omega)n_i(\omega+\nu) = I(\omega) \tag{14}$$

with

$$X(\omega) = \omega^2 - 1 + \sum_{j=1}^{2} g_j{}^2\nu_j / (\omega^2-\nu_j{}^2)$$

$$Y_\pm(\omega) = \frac{(\nu_1+\nu_2)g_1g_2}{2(\omega\pm\nu_1)(\omega\mp\nu_2)} \tag{15}$$

$$g_j{}^2 = \chi\,(M\chi/16m)^{1/2}\lambda_j{}^2$$

Eq. (14) also follows directly from Eq. (25) of Arnush et al.[1], derived from the Vlasov equation, provided we take the fluid limit for the $\varepsilon(\underline{k}, \omega)$ in their equation. The right hand side of (14) involves the initial conditions on $n_i(\tau)$ and its derivatives, but we can simply set it equal to zero in finding the dispersion relation. Thus, vanishing of the determinant D of the coupled equations (14)

$$D = \det \begin{bmatrix} \ddots & \ddots & \ddots & & & \\ & Y_-^{(-1)} & X^{(-1)} & Y_+^{(-1)} & & \\ & & Y_-^{(0)} & X^{(0)} & Y_+^{(0)} & \\ & & & Y_-^{(1)} & X^{(1)} & Y_+^{(1)} \\ & & & & \ddots & \ddots & \ddots \end{bmatrix} = 0 \tag{16}$$

yields the dispersion relation, where $X^{(n)} \equiv X(\omega+n\omega)$ and similarly for $Y_\pm^{(n)}$. (Note that the matrix of eq. (16) is tridiagonal.)

Before discussing the solution of (16) we examine the Mathieu-like equation derived from the system (11) through (13). Differentiating (11) twice and (12) and (13) once allows us to eliminate $f_\pm$ and obtain a fourth order

equation for n_i

$$S\, n_i^{(4)} - S^{(1)}\, n_i^{(3)} + (S+H)\, n_i^{(2)} - S^{(1)}\, n_i^{(1)} + (CS^2+H)\, n_i = 0 \qquad (17)$$

where $C = (M\chi/m)^{1/2}(\chi/8)$, the upper script (j) indicates the jth derivative with respect to τ and S and H are periodic functions of $\nu\tau = (\nu_1-\nu_2)\tau$:

$$S = 2[\sum \nu_j\, \lambda_j^2 + \lambda_1\lambda_2(\nu_1-\nu_2)\cos\nu\tau]$$

$$H = 2[\sum \nu_j^3\, \lambda_j^2 + \lambda_1\lambda_2\nu_1\nu_2(\nu_1+\nu_2)\cos\nu\tau]$$

Because of the S^2 term in the coefficient of n_i, the Laplace transform of this equation couples $n_i(\omega)$ not only to $n_i(\omega\pm\nu)$ but also to $n_i(\omega\pm2\nu)$, i.e. we get a 5 term recursion relation rather than (14). For this reason, it is more convenient to work instead with a sixth order equation for n_i whose coefficients involve only $\cos\nu\tau$ and $\sin\nu\tau$ but not the harmonics of ν. This equation can be obtained by operating on (11) with the two operators

$$L_j = (d/d\tau)^2 + \nu_j^2 \qquad j = 1, 2 \qquad (18)$$

and using Eqs. (12) and (13) to simplify the terms on the right side. The result is

$$[L_1L_2L + (g_1^2\nu_1L_2 + g_2^2\nu_2L_1)]\, n_i =$$

$$-(\nu_1+\nu_2)\,\frac{(g_1g_2)}{2}\,[L_2^-\, L_1^+\{\exp(i\nu\tau)n_i\} + L_2^+\, L_1^-\{\exp(-i\nu\tau)n_i\} \qquad (19)$$

where

$$L = (d/d\tau)^2 + 1 \qquad L_j^{\pm} = (d/d\tau \pm i\nu_j) \qquad (20)$$

Of course, the Laplace transform of Eq. (19) gives just Eq. (14).

Equation (19) is an interesting generalizaton of the Mathieu equation, which we can write as

$$\frac{\partial^2 n}{\partial \tau^2} + \quad + g^2 n \cos\nu\tau = 0 \tag{21}$$

Indeed, the Laplace transform of (21) gives a system of equations identical to (14) but with X, $Y_{\pm}$ replaced by

$$\tilde{X}(\omega) = \omega^2 - 1$$
$$\tilde{Y}_{\pm}(\omega) = - g^2/2 \tag{22}$$

and an analysis of that system leads to the usual Mathieu stability diagram. A comparison of (19) and (21) is instructive. If the right side of (21), i.e. the part with periodic coefficients, vanishes, the dispersion equation reduces to $\tilde{X}(\omega) = 0$, which has only the stable solutions $\omega = \pm 1$. On the other hand, even if the right hand side of Eq. (19), i.e., the part with periodic coefficients, vanishes, the resulting dispersion equation (14), $X(\omega) = 0$, has both stable and unstable roots. Indeed, with $g_2 = 0$ (which makes the right side of (19) vanish) $X(\omega) = 0$ is just the usual dispersion for single pump parametric instabilities

$$(\omega^2-1)(\omega^2-\nu_1^2) + g_1^2\nu_1 = 0 \tag{23}$$

This has unstable roots for

$$g_1^2 > (\nu_1^2-1)^2/4\nu_1 \quad \text{or} \quad 0 < -\nu_1 < g_1^2 \tag{24}$$

corresponding to the parametric decay and the OTSI, respectively. More generally, $X(\omega) = 0$ has unstable solutions for given ν_1, ν_2 if g_1 exceeds certain threshold levels. This corresponds to one mechanism for instability, which may be considered as a straightforward extension of the usual parametric in-

stabilities (decay and OTSI), and is quite different from the situation in the ordinary Mathieu equation, where there is no instability in absence of the term with a periodic coefficient.

The second (Mathieu-like) mechanism is evident when g_1 is below the threshold for instabilities arising from $X(\omega) = 0$, since Eq. (19) for $g_2 \neq 0$ can still have instabilities due to the terms on the right hand side with periodic coefficients. This instability mechanism is clearly analogous to that associated with the Mathieu equation, where instabilities arise only from the g^2 term in (21). In general, for arbitrary g_1 and g_2 we have the presence of both instability mechanisms.

III. ANALYSIS OF THE DISPERSION EQUATION

In this section we solve the dispersion equation (15) using Hill's method. We also discuss an approximation which provides some physical insight and which proves to be quite accurate in the parameter regime of greatest interest. The approximation is based on an expansion in the quantity $g = (g_1 g_2)^{1/2}$ which we treat as a small parameter.

For arbitrary g we define a new determinant $\tilde{D}$ obtained by dividing D by its diagonal elements

$$D(\omega) = \tilde{D}(\omega) \prod_{n=-\infty}^{\infty} X^{(n)}(\omega)$$

$$\tilde{D}(\omega) \equiv \begin{bmatrix} \ddots & \ddots & \ddots & & & & \\ \ddots & \ddots & \ddots & & & & \\ \ddots & \ddots & \ddots & & & & \\ & & & W_-^{(-1)} & 1 & W_+^{(-1)} & \\ & & & & W_-^{(0)} & 1 & W_+^{(0)} \\ & & & & & W_-^{(1)} & 1 & W_+^{(1)} \\ & & & & & \ddots & \ddots & \ddots \\ & & & & & \ddots & \ddots & \ddots \\ & & & & & & \ddots & \ddots & \ddots \end{bmatrix} \qquad (25)$$

where

$$W_{\pm}^{(n)} = Y_{\pm}^{(n)}(\omega)/X^{(n)}(\omega)$$

is of order g^2. If g is small, we can expand $\tilde{D}$ in powers of g:

$$\tilde{D}(\omega) = 1 + \sum_{n=-\infty}^{\infty} W_+^{(n)}(\omega)\, W_-^{(n+1)}(\omega) + O(g^6) \qquad (26)$$

In the limit $g = 0$, $\tilde{D} = 1$ but D can still vanish, namely if ω is a root of $X^{(n)}(\omega)$. For later use we define the quantities r_i, i = 1 to 6, as the roots of $X(\omega)$, for arbitrary g_1 and g_2,

$$X(r_i) = r_i^2 - 1 + \sum_j g_j^2 \nu_j (r_i^2 - \nu_j^2)^{-1} = 0 \qquad (27)$$

In general, the roots r_i have no simple physical significance, but we note the following properties. If $g_1 \neq 0$ and $g_2 = g = 0$, then Eq. (27) is a biquadratic in ω whose roots give the usual single pump parametric instabilities as illustrated in Fig. 1 for $g_1 = .346$. (The points A, P, M shown in Fig. 1 are used later in the discussion of Fig. 5.). In the stable region $|\nu_1 - 1| > g_1$ there are two real roots, the ion acoustic mode with $\omega \simeq 1$, and what we may call the pump idler mode, with $\omega \simeq \nu_1$. If g_1 and g_2 are both non-zero, Eq.(27) is a cubic in ω^2 whose roots are, for small g_j, close to $\omega^2 = 1$ (normal ion acoustic modes, present even if $g_j \to 0$) and to $\omega^2 = \omega_1^2$ and $\omega^2 = \omega_2^2$ (pump modes or idlers, which have no physical significance in the limit $g_j \to 0$).

We now consider the roots of $\tilde{D}(\omega)$ for small g. Since the second term in $\tilde{D}$ is of order g^4, $\tilde{D}$ can vanish only if one or more of the $X^{(n)}(\omega)$ is small, i.e. if $(\omega + n\nu)$ is near 1, corresponding to an ion acoustic resonance. Of particular interest is the case when two of the $X^{(n)}$ vanish simultaneously, which can happen, with $\nu \neq 0$, if, for two integers n_1, and n_2,

$$\omega + n_1\nu \simeq 1 \qquad \omega + n_2\nu \simeq -1 \qquad (28)$$

i.e. if

$$\nu \simeq 2/N \qquad (29)$$

where N is an integer. Of special interest is the case of "double resonance" where one of the terms in $\tilde{D}$ involves the product of <u>two</u> large W factors, e.g. when

$$\omega \simeq -1 \qquad \omega + \nu \simeq 1 \qquad (30)$$

which requires $\nu \simeq 2$, $N = 1$. The most interesting results are obtained in this case, which can be understood on physical grounds as follows. From the differential equation (19) we see that the ions are driven by a ponderomotive

force of frequency ν, so a low frequency wave at ω gives rise to another, at frequency $\omega-\nu$. Both waves can be normal modes if $\omega \simeq 1$, $\nu \simeq 2$ so that $\omega - \nu \simeq -1$, giving the condition of "double resonance". For $N > 1$ this double resonance cannot occur so the effects of the second pump are less pronounced. However, the case $N \simeq 2$, $\nu \simeq 1$ is of some interest. A wave at $\omega \simeq 1$ then gives rise, through the ponderomotive force, to a wave at $\omega \simeq 1-\nu \simeq 0$, and while this is not a normal mode, it does correspond to an OTSI mode. The thresholds for this case are discussed in Arnush et al.[1]

Having seen where the most interesting effects are likely to occur, we consider the exact solution of the dispersion equation (15), i.e. without assuming g small. The determinant $\tilde{D}(\omega)$ defined by Eq. (25) has the following properties:

a) $\tilde{D}(\omega + \nu) = \tilde{D}(\omega)$

b) $\lim_{\omega\to\infty} \tilde{D}(\omega) = 1$ since $\lim_{\omega\to\infty} W_{\pm}^{(n)}(\omega) = 0$

c) $\tilde{D}(\omega) = \tilde{D}(-\omega) = \tilde{D}^*(\omega^*)$

Since $X^{(n)}(\omega)$ vanishes at $\omega = r_i^{(n)} \equiv r_i + n\nu$ where r_i are the 6 roots of $X(\omega)$, $\tilde{D}(\omega)$ has poles at $r_i^{(n)}$. These will be simple poles provided we avoid the special ν values where $r_i - r_j = p\nu$ for some integer p. Then the function

$$K(\omega) \equiv \tilde{D}(\omega) - \sum_{i=1}^{\infty} \sum_{n=-\infty}^{\infty} b_{i,n}(\omega - r_i^{(n)})^{-1} \tag{31}$$

where $b_{i,n}$ is the residue of $\tilde{D}$ at $r_i^{(n)}$, will be analytic in the whole ω plane and since $K \to 1$ as $\omega \to \infty$, we have $K = 1$. The periodicity of $\tilde{D}$ implies that the residues at $r_i^{(n)}$ and $r_i^{(m)}$ must be the same, i.e. that $b_{i,n} = b_i$ independent of n. Finally,

$$\sum_{n=-\infty}^{\infty} (\omega - r_i^{(n)})^{-1} = \sum_{n=-\infty}^{\infty} \nu^{-1}[n-(\omega-r_i)/\nu]^{-1} = (\pi/\nu)\cot[\pi(\omega-r_i)/\nu] \tag{32}$$

so

$$\tilde{D}(\omega) = 1 + \sum_{i=1}^{6} (b_i\pi/\nu)\cot[\pi(\omega-r_i)/\nu] \tag{33}$$

The symmetry of both $\tilde{D}$ and X under $\omega \to -\omega$ means that if we arrange the roots r_i so that $r_{i+3} = -r_i$, $i = 1,2,3$, then $b_{i+3} = -b_i$ and the dispersion relation takes the form

$$\tilde{D}(\omega) = 1 + \sum_{i=1}^{3} (b_i\,\pi/\nu)\{\cot[\pi(\omega-r_i)/\nu] - \cot[\pi(\omega+r_i)/\nu]\} = 0 \tag{34}$$

Since (34) gives the dependence of $\tilde{D}$ on ω in explicit form, it is easy to determine the roots of $\tilde{D}$ once the b_i are known as functions of ν. Note that the method fails when $\nu = 0$ since the single poles $r_i^{(n)}$ converge into a single point giving rise to an essential singularity. Therefore the neighborhood of $\nu = 0$ is excluded in our numerical calculations. However, $\nu = 0$ implies that both pumps have the same frequency and the corresponding growth rate is expected to be that of a single coherent pump whose amplitude is the sum of the two pump amplitudes.

The r_i's are poles of $\tilde{D}$, so the residues, b_i, are given by

$$b_i = \lim_{\omega \to r_i} \tilde{D}(\omega)(\omega - r_i) \tag{35}$$

These infinite determinants can conveniently be evaluated using iteration:

$$\frac{D_{n+1}}{D_n} = a_{n+1,n+1} - \frac{a_{n,n+1}a_{n+1,n}}{(D_n/D_{n-1})} \tag{36}$$

where D_n is the approximate value of $\tilde{D}$ obtained from an $n \times n$ truncation and $a_{n+1,n+1}$, $a_{n,n+1}$, $a_{n+1,n}$ are the elements of the (n+1)th row and column. Al-

though some of the $a_{n,m}$ are singular at $\omega = r_i$ due to the vanishing of $X(\omega)$ factors which appear in the denominator, $(\omega-r_i)a_{n,m}(\omega)$ is always finite. The iteration scheme converges fairly well; typically, for values of ν bigger than 0.5, 10 iterations suffice to give an accuracy of 0.1%.

The roots of $\tilde{D}$ obtained by this procedure are plotted as functions of the parameters ν_1, ν_2, etc. as discussed, with illustrative examples, in Sec. IV. To understand the considerable structure which results, the following approximate treatment of the double resonance case proves helpful. For $\nu \simeq 2$, $\omega \simeq 1$ we have, to order g^4, keeping only the largest resonant terms,

$$\tilde{D} \simeq 1 + W_+(\omega-\nu)\, W_-(\omega) = 1 + Y_+(\omega-\nu)\, Y_-(\omega)/X(\omega-\nu)\, X(\omega) = 0 \qquad (37)$$

This equation, which is equivalent to approximating $\tilde{D}$ by a 2×2 determinant, gives an eighth degree polynomial in ω, when rationalized, but it can be reduced to a biquadratic in the limit $\nu_1 \simeq -\nu_2 \simeq 1$. Since

$$X(\omega) \simeq (\omega^2-1) + g_1^2/2(\omega-\nu_1) - g_2^2/2(\omega+\nu_2)$$

$$X(\omega-\nu) \simeq \{(\omega-\nu)^2 - 1\} - g_1^2/2(\omega+\nu_2) + g_2^2/2(\omega-\nu_1)$$

$$Y_+(\omega-\nu) = Y_-(\omega) = (\nu_1+\nu_2)(g_1g_2)/2(\omega-\nu_1)(\omega+\nu_2),$$

the change of variable

$$\omega = \nu/2 + y \qquad (38)$$

gives a cubic in y^2,

$$(y^2-d^2)(y^2-a^2)(y^2-b^2)+(g_1^2+g_2^2)b(y^2+ad)-(g_1^2-g_2^2)\nu y^2-(1/4)(g_1^2-g_2^2)^2 = 0 \qquad (39)$$

where $a = (\delta_1 - \delta_2)/2$, $b = (\delta_1 + \delta_2)/2$, $\delta_1 = \nu_1 - 1$ and $\delta_2 = \nu_2 + 1$ are small quantities in the double resonance regime and $d = \nu/2 + 1$, with $d \simeq 2$ in that regime. If the growth rate γ and the shift in the normal mode frequency, $(\mathrm{Re}\omega - 1)$, are much smaller than 1, as is the case for small amplitude pumps, then $|y|^2 \ll d^2$ for $\nu \simeq 2$ and equation (39) becomes

$$y^4 - 2Ay^2 + B = 0 \tag{40}$$

where

$$\begin{aligned} A &= \frac{1}{2}\{a^2+b^2+(g_1^2+g_2^2)b/d^2-(g_1^2-g_2^2)\nu/d^2\} \\ B &= a^2b^2 + (g_1^2-g_2^2)^2/4d^2 - (g_1^2+g_2^2)ab/d \end{aligned} \tag{41}$$

From (38) and (40) we have

$$\omega = \nu/2 + [A + (A^2-B)^{1/2}]^{1/2} \tag{42}$$

as a convenient closed form approximation for the roots of $\tilde{D}(\omega)$ which is valid for $\nu_1 = -\nu_2 \simeq 1$ and small values of g_j. (Note that (42) gives four roots since each square root can have either a positive or negative sign.)

The rather complicated dependence of the growth rate on the pump frequencies and amplitudes as determined from the numerical solution of (34) can be understood in a fairly simple way from an examination of (41) and (42), which actually provide a good approximation even when δ_1 and δ_2 are not small. From (42) we can see that there are two disjoint conditions for instability

a) $B < 0$ (43)

b) $B > A^2$ (44)

and the boundaries between the stable and unstable regions of parameter space are then determined by the locii $B = 0$ and $B = A^2$, as shown in Fig. 2. We first note that the number of unstable roots of (42) varies from 0 to 2 according to the signs of A, B and $A^2 - B$. The various possibilities are summarized in Fig. 2.

We may say that region a) represents the generalized Mathieu instability since Re ω is locked to one half of the (ponderomotive force) driving frequency, $\nu/2$, just as in the lowest unstable mode of the usual Mathieu equation. Similarly, we may consider region b) as the generalization of the single pump decay instability since in the limit $g_2 \to 0$, $\nu_2 \to -1$, we have $B = A^2$ and (42) reduces to the usual single pump expression

$$\omega = \nu/2 \pm A^{1/2} + \{1 + \nu_1 \pm [(1-\nu_1)^2 - g_1^2\nu_1]^{1/2}\}/2, \tag{45}$$

unstable if $g > g_s = (1-\nu_1)\nu_1^{-1/2}$.

The mapping of the stability boundaries on the physical space of the parameters can be obtained by examining the surfaces $B = 0$ and $B = A^2$ which characterize the different regions of Fig. 2. Since there are four independent parameters (ν_1, ν_2, g_1 and g_2) it is convenient to fix two of these and plot the curves $B = 0$ and $B = A^2$ in the plane of the remaining two parameters. Examples of such plots are shown in Fig. 3 with the respective regions of Fig. 2 identified.

IV. SOLUTIONS OF THE DISPERSION RELATION

In this section we analyze the roots of (34) as functions of the parameters ν_1, ν_2, E_1 and E_2. Numerical calculations of both growth rates and frequencies, are presented and the approximate form of the dispersion equation (42) is used to analyze the resulting structure.

The new effects resulting form the presence of the second pump are most evident at resonance, i.e., when one of the pump frequencies differs from the Bohm-Gross frequency by approximately Ω_k, the ion acoustic frequency. We shall therefore consider two cases:

i) $\nu_1 \simeq 1$, ν_2 arbitrary

ii) $\nu_2 \simeq -1$, ν_1 arbitrary

i) $\nu_1 \simeq 1$

We begin with the case of equal amplitude pumps $g_1 = g_2 = g$, with g well above the single pump decay instability threshold, $g_s \simeq (\nu_1-1)\nu_1^{-1/2} \simeq \delta_1$. Of the various roots of (34) we select the ion acoustic wave, i.e., the one with $\gamma = \text{Im}\ \omega > 0$ which has $\text{Re}\ \omega \simeq 1$ (in units of Ω_k). In Fig. 4 we show γ and $\text{Re}\ \omega$ as a function of ν_2 for $\nu_1 = 1.1$ and $g_1 = g_2 = g = 0.346$. (The region $\nu_2 \simeq \nu_1$ is excluded from the plot for the reason stated in Sec. III. Note that the growth rate increases as we approach $\nu_2=\nu_1$, consistent with our expectation that $\gamma \to 2\gamma_s$ at that point).

For most values of ν_2, we see that $\gamma \simeq \gamma_s \simeq [\nu_1(g^2-g_s^2)]^{1/2}$, the single pump decay instability growth rate, i.e., the second pump has little effect. The enhancement of γ when $\nu_2 \simeq 0$ is not unexpected, since the second pump could then produce the oscillating two stream instabiltiy (OTSI) even in the absence of the first pump. Actually, close inspection of Fig. 4 shows that γ

is enhanced for both positive and negative values of ν_2, whereas the usual OTSI instability arises only for a pump frequency below the Bohm-Gross frequency. However, the most striking feature of Fig. 4 is the total supression of the instability for $\nu_2 = -\nu_1$ and $\nu_2 = \pm(2-\nu_1)$, arising from the interaction between the two mechanisms, parametric and Mathieu-like, discussed in Sec. I.

An understanding of the structure of Fig. 4 can be obtained from the approximate solution of (34) given by (42). For equal pump powers not too far above threshold, A is positive, since δ_1, δ_2 and $g_1 = g_2 = g$ are all small quantities of the same order and hence the $(a^2 + b^2)$ term in A dominates. Therefore, condition (43) for the generalized Mathieu instability becomes, with $d \simeq 2$,

$$(ab)^2 - g^2 ab > 0 \tag{46}$$

which is equivalent to

$$0 < \delta_1^2 - \delta_2^2 < 4g^2 \tag{47}$$

In Fig. 4, $g > \delta_1$ so the right half of (47) is automatically satisfied. The condition $|\delta_2| < |\delta_1|$ just corresponds to the region between the nulls marked 1 and 2 in Fig. 4. In this region, we find that, as expected from (42), Re ω is locked to $\nu/2$. At the ends of that interval we have $\delta_1 = \pm\delta_2$, i.e.,

$$\begin{aligned} \nu_2 &= -\nu_1 \quad \text{or} \quad b = 0 \\ \nu_1 - \nu_2 &= 2 \quad \text{or} \quad a = 0 \end{aligned} \tag{48}$$

Since (48) is independent of the pump amplitude, these are stable points of the system and can not be excited even if the pump amplitude is increased (subject, of course, to the small pump amplitude assumption which un-

derlies our whole analysis).

We note that the nulls at 1 and 2 in Fig. 4 correspond to a certain symmetry in the frequency spectrum. For $\nu_2 = -\nu_1$, the pumps are symmetrically placed above and below the Bohm-Gross frequency, resulting in a cancellation similar to that which occurs if a harmonic oscillator is driven by equal amplitude pumps symmetrically located above and below its resonant frequency. The existence of this null has also been noted by Fejer et al.[5] For $\nu_1 - \nu_2 = 2$, corresponding to the null at 2, the symmetry manifests itself at low frequencies, as follows. A low frequency fluctuation, at frequency ω, beating with the pump at ω_1 gives rise to a sideband at $\omega_1 - \omega$, the interaction being strongest when the sideband is resonant, i.e., when $\omega_1 - \omega = \omega_k$ or $\omega = \nu_1$. The sideband at $\omega_1 - \omega$, beating with the second pump, produces a low frequency oscillation at $(\omega_1 - \omega) - \omega_2 = \nu - \omega = \nu - \nu_1 = -\nu_2$. Double resonance occurs when both of the low frequency signals are near the ion acoustic frequency, Ω_k, i.e. $\nu_1 \simeq -\nu_2 \simeq 1$. When $\nu_1 - \nu_2 = 2$, we have $\nu_1 - 1 = 1 - (-\nu_2)$, i.e., the two low frequency signals are located symmetrically above and below Ω_k and there is a cancellation. This same situation arises when both pumps are above the Bohm-Gross frequency, $\nu_1 \simeq \nu_2 \simeq 1$ and $\nu_1 + \nu_2 = 2$ or $\nu_1 - 1 = 1 - \nu_2$. The resulting cancellation accounts for the null denoted as 3 in Fig. 4.

While the nulls in Fig. 4 arise from these symmetries, the first two being associated with the double resonance condition $N = 1$, $\nu \simeq 2$, the slight enhancements in γ correspond to other values of N. Those for $N = 2$ and $N = -1$ are clearly visible (at $\nu_2 \simeq \nu_1 - 1$ and $\nu_2 \simeq \nu_1 + 2$, respectively) and the $N = 3$ peak (at $\nu_2 \simeq \nu_1 - 2/3$) is barely visible on the scale used for display. Higher order interactions ($N > 3$ and $N < -1$) would appear for larger values of

g. As a final comment on this equal amplitude case, we note that if the first pump is exactly on resonance, $\nu_1 = 1$, then $a = -b$; the two conditions (48) are the same; the two nulls at 1 and 2 coalesce; and there is no Mathieu-like behavior.

In discussing other values of the parameters, we shall concentrate on the N = 1 (double resonance) case, where the most striking effects occur. Also, we will plot Re ω and γ for all of the four modes with Re ω of order 1. In general, we plot only the positive γ values but, of course, for each root of the dispersion equation with $\gamma > 0$ there is another with imaginary part equal to $-\gamma$. If we keep the pump amplitudes equal, $g_1 = g_2 = g$ but put g below the parametric instability threshold g_s for the first pump acting alone, we obtain the results shown in Figs. 5a, 5b and 5c. In Fig. 5a, $g < \delta_1/2$ and it follows from (47) that the range of instability δ_2 is not the whole interval $-\delta_1 \leq \delta_2 \leq \delta_1$ as in Fig.4 but instead only the portion

$$(\delta_1^2 - 4g^2)^{1/2} \leq |\delta_2| \leq \delta_1 \tag{49}$$

This corresponds to the two growth regions in Fig. 5a. In Figs. 5b and 5c, $\delta_1/2 < g < \delta_1$. In this case, the instability region for δ_2 expands to the whole interval $(-\delta_1, \delta_1)$. Finally, in Fig. 5d, $g > \delta_1$, we obtain the Mathieu instability on the interval $(-\delta_1, \delta_1)$ and the decay instability when ν_2 is far from -1. The behavior of both γ and Re ω in these figures is consistent with the characterization of the roots of (40) given in Fig. 2. In Fig. 5a as we move from left to right we are first in region IV of Fig. 2, then in regions I, IV, I and IV. In Figs. 5b and 5c we have that the central feature corresponds to region I and the sides to region IV. in Fig. 5d, again moving from left to right we go through regions III, IV, I, IV and III.

An alternative view of the structure of Fig. 5 is as follows. For Figs. 5a, 5b and 5c where $g_1 < g_s$ (for a given value of ν_1) there would be, in absence of the second pump, two stable modes, the ion acoustic, with $\omega \simeq 1$ (point A in Fig. 1) and the "pump" mode, with $\omega \simeq \nu_1$ (point P in Fig. 1). The ponderomotive force with frequency ν may interact with either of these, instability occuring if the beat wave resulting from this interaction is also resonant. This occurs, for example, when $\nu - \nu_1 \simeq \nu_1$, i.e. for $\nu_2 \simeq -\nu_1$, corresponding to the left hand bump in Fig. 5a. Similarly, $\nu - 1 \simeq 1$ or $\nu_2 \simeq \nu_1 - 2$ corresponds to the right hand bump. As g increases, point M in Fig. 1 moves closer to ν_1 (since the width of the instability region is proportional to g) and the ion acoustic and pump mode can be coupled through the action of the ponderomotive force, resulting in the γ variation shown in Figs. 5b and 5c. Finally, for $g > g_s$ point M has moved to the right of ν_1, giving growth for most values of ν_2 save for the interval where the Mathieu mechanism dominates and is stabilizing (Fig. 5d).

For unequal pump amplitudes, we find similar dependences of the roots of (34). If the amplitude of the first pump is below the single pump instability threshold, $g_1 < \delta_1$, we obtain the results shown in Fig. 6 for $g_1 = .075$. For $g_2 = g_1/3$ (Fig. 6a), there are two disjoint regions of growth within the interval $|\delta_2| < |\delta_1|$ whereas for larger g_2 these merge into a single region (Figs. 6b and 6c). To understand this structure, we note that since $g_1 < \delta_1$, we have $A > 0$ and the condition for the Mathieu instability is just (43), which can be written in the form

$$\delta_1^2 - (g_1 + g_2)^2 < \delta_2^2 < \delta_1^2 - (g_1 - g_2)^2 \tag{50}$$

If $g_2 < \delta_1 - g_1$, (50) predicts two disjoint instability regions, as in

Fig. 6a. If $\delta_1 - g_1 < g_2 < \delta_1 + g_1$, then the left half of (50) is automatically satisfied and there is only one region of instability, whose boundaries are within the interval $|\delta_2| < |\delta_1|$, as in Figs. 6b and 6c. If $g_2 > \delta_1 + g_1$, then (50) cannot be satisfied and there is no Mathieu instability, i.e., we have crossed from region I in Fig. 2 to region IV. The qualitative view given previously for Fig. 5 also applies to the conditions of Fig. 6.

If, instead, the first pump amplitude is above the single pump decay threshold, $g_1 > \delta_1$, then A may be either positive or negative. In Fig. 7a, where $g_1 \simeq 1.7\ \delta_1$ and $g_2 = g_1/2$ we pass from region I of Fig. 2, when ν_2 is near -1, through region II ($A < 0$) and eventually to region III, at either side of ν_2=-1. Although the decay instability growth rate is somewhat modified by the presence of the second pump, g_2/g_1 is so small that there is no region of ν_2 where the instability is completely suppressed. If $g_2 > g_1$, then it follows directly from (41) that $A > 0$ and instability can occur only in regions I and III of Fig. 2. This situation is illustrated in Fig. 7b, where $g_1 = 1.7\ \delta_1$ as in Fig. 7a but $g_2 = 1.1\ g_1$. For these values, (50) predicts a single instability region around $\nu_2 = -1$, as seen in Fig. 7b, since $g_2 < \delta_1 + g_1$. As ν_2 decreases, we pass from region I through the stable region IV and eventually come to the decay instability (region III) near $\nu_2 = -1.5$ (We pass through these same regions as ν_2 increases from -1 to -0.5).

We see from (50) that as the second pump amplitude increases, we eventually supress the Mathieu instability since for $g_2 > g_1 + \delta_1$ the condition $B < 0$ cannot be satisfied. Thus, as g_2 increases from 0 to $g_1 + \delta_1$, the maximum growth rate for the Mathieu instability (which occurs at $\delta_2 \simeq 0$) for given ν_1 and g_1, increases, reaches an optimum, and then decreases, as shown in Fig. 6.

ii) $\nu_2 \simeq -1$

We consider here only the regime $\nu_1 > 0$, i.e., we study the modification

of the decay instability due to the first pump. Some typical results are plotted in Fig. 8. For comparison the single pump case ($g_2 = 0$) is shown in Fig. 1. In Figs. 8a and 8b the pump amplitudes are equal, $g_1 = g_2 = g = .346$ so $A > 0$ and instability can arise only from regions I and III of Fig. 2. For $\nu_2 = -1$, we have

$$B = \delta_1^2(\delta_1^2 - 4g^2)/16 \tag{51}$$

hence the Mathieu instability occurs over the interval $|\delta_1| < 2g$, as shown in Fig. 8a. The vanishing of the growth rate at $\nu_1 = 1$ is a consequence of the symmetrical location of the pumps above and below the Bohm-Gross frequency, as discussed earlier. When ν_2 is displaced from -1, e.g., $\nu_2 = -1.2$ as in Fig. 8b, we have

$$B = (\delta_1^2 - \delta_2^2)(\delta_1^2 - \delta_2^2 - 4g^2)/16 \tag{52}$$

Thus the Mathieu instability (associated with $B < 0$) occurs for

$$\delta_1^2 - 2g^2 < \delta_2^2 < \delta_1^2 \tag{53}$$

This corresponds to the right-hand and left-hand bumps in γ in Fig. 8b. Outside of the interval (53) the Mathieu instability does not occur, but between the two bumps B becomes larger than A^2 and we encounter the decay instability (region III of Fig. 2) as evidenced by the central bump in Fig. 8b.

For different pump amplitudes, we observe various combinations of the Mathieu and decay instabilities. Fig. 8c shows a case where $A > 0$ (since $g_2 > g_1$) and we move from region IV, for $\nu_1 \approx 0$, to regions I, IV, III, IV, I and IV as ν_1 increases up to 2. For $g_2 < g_1$, as in Fig. 8d, we cannot predict the sign of A from simple arguments. In general it will depend on the values

of g_1, g_2, and ν_1, but for the parameters of Fig. 8d, it is clear, from the behavior of both γ and Re ω, that as ν_1 increases from 0 to 2 we pass, successively, through regions IV, I, II, III, II, I and IV.

From Fig. 3 it is easy to follow the path through the stability plane corresponding to the curves of Figs. 5 through 8. For example, Fig. 8d corresponds to the dotted horizontal line at $g_2 = g_1/2$ shown in Fig. 3d.

In all of the discussions of this section, we have used the approximate solution (42) of the dispersion equation to explain the results obtained numerically from the exact equation (34). This is justified by the close agreement of the exact and approximate solutions when δ_1 and δ_2 are not too large. This agreement is illustrated for typical values of the parameters in Fig. 9, where the solid line corresponds to the the solutions of the exact dispersion (34) and the dotted line to the approximation (42). Note that in this figure we have plotted the growth rates for all roots, i.e., those with $\gamma < 0$ are also included.

V. TIME DOMAIN BEHAVIOR

Although the stability properties of our basic equations (10) through (12) are fully described by the frequency domain analysis presented in the previous two sections, additional physical insight can be obtained by examining the time domain solutions of these equations. We use a fourth order Runge-Kutta technique[6] to solve the fourth order system (10) through (12), taking as initial condition a standing ion acoustic wave [$f_+(0) = f_-(0) = 0$; $n_i(0) = 1$; $\dot{n}_i(0) = 0$]. The integration is done using a step size $\Delta t = 0.4$ (in units of Ω_k^{-1}) for 256 steps. The result is unchanged when Δt is taken to be 0.1. We also calculated frequency spectra from these solutions using a fast Fourier transform[7] with 256 sample points. Insofar as the nonlinear mechanisms responsible for saturation of the instability are weakly dependent on frequency, these spectra are representative of what might be seen in an actual experimental measurement of the frequency spectrum of the ion or electron density fluctuations. Of course, the fine details of the spectrum, e.g., the ratios of the various spectral peaks depend somewhat upon the precise initial conditions, such as the ratio of left-going and right-going ion acoustic waves and/or Langmuir waves.

Fig. 10 shows the results for a choice of parameters ($\nu_1 = 1.1$, $\nu_2 = -0.8$[8], $g_1 = g_2 = .346$) corresponding to a point just to the right of null 2 in Fig. 4. Since this is in region III of Fig. 2, the dispersion relation predicts two modes with equal growth rate and different Re ω. The beating of these two modes causes the modulation in $n_i(t)$ shown in Fig. 10a. (The existence of the two modes is also apparent from the plot of $|n_i(\omega)|^2$ in Fig. 10c.) The exponential growth of the two modes (following an initial transient period) is reflected in the plot of $\log|n_i|$ in Fig. 10b.

In Fig. 11 we show $n_i(t)$ for parameters chosen to correspond to the nulls 1, 2 and 3 in Fig. 4. In each case there is a modulation but, as expected, no net growth. When $\nu_1 = -\nu_2$ (as in Fig. 11a) we note that (11) through (13) reduce to

$$\partial(f_+ + f_-)/\partial\tau = 0$$
$$\partial^2 n_i/\partial\tau^2 + n_i = -i(\chi/2)[f_+(0) + f_-(0)]\lambda \cos \nu_1\tau \tag{54}$$

from which it is obvious that n_i is a superposition of oscillations at $\omega = 1$ and $\omega = \nu_1$, resulting in the modulation seen in Fig. 11a.

In experimental observations, especially in the case of the ionosphere, the most accessible quantity is the electron density $n_e(\omega)$ at high frequencies (of order of the Bohm-Gross frequency), measured, for example, by Thomson scattering. In Fig. 12 we show the spectral distributions $|n_e(\omega)|^2$ obtained by fast Fourier transform of the direct solutions of (10) through (12) for equal amplitude pumps $g_1 = g_2 = .346$ with $\nu_1 = 1.1$ and various values of ν_2. The locations of the two pumps are indicated with dotted lines and the amplitudes $|n_e(\omega)|^2$ are arbitrarily normalized to the largest value found in this set, which occurs in Fig. 12g. Of course, the various peaks of the high frequency electron density spectrum just correspond to peaks in the low frequency ion density spectrum, which is shown, for the same parameters, in Fig. 13; indeed it follows from (12) that

$$-i\omega f_+(\omega) = f_+(t=0) - (M\chi/m)^{1/2}[\lambda_1 n_i(\omega-\nu_1) + \lambda_2 n_i(\omega-\nu_2)]/4 \tag{55}$$

For $\nu_1 = 1$ and ν_2 far from -1, as in Figs. 12a, 13a, the spectrum is dominated by the single pump decay associated with the first pump. As ν_2 approaches -1 the spectrum becomes modified (Figs. 12b,c and 13b,c). For $\nu_2 = -1$, we are in region I of Fig. 2, so there is one unstable root for Re $\omega > 0$ (and another

for Re $\omega < 0$) in $n_i(\omega)$ and hence four (two coinciding at $\omega = \omega_k$) for $n_e(\omega)$. For $\nu_2 = -0.88$ (Figs. 12d, 13d) we are in region III of Fig. 2 and the two unstable modes (for Re $\omega > 0$) in $n_i(\omega)$ result in a splitting of the $n_e(\omega)$ peaks. As ν_2 continues to increase (Figs. 12e through 12h and 13e through 13h) the spectrum of $n_e(\omega)$ again resembles the single pump decay, with various modifications in the line shape.

VI. CONCLUSIONS AND DISCUSSION OF RESULTS

Our study of the effect of a second pump on the parametric instability growth rate of ion acoustic and Langmuir waves is valid for long wavelength pumps in a uniform medium, i.e. for $L_n > \lambda_p > \lambda_w$ where L_n is the density gradient scale length, λ_p is the pump wavelength and λ_w is the wavelength of the waves excited by the parametric process.

New effects appear in the case of two pumps because, in addition to the constant term produced by a single pump, which results in the usual parametric instabilities, the ponderomotive force contains also an oscillating term of frequency $\Delta = \omega_1 - \omega_2$. This gives the ion density equation a character similar to the Mathieu equation, although the differential equation arising here is of higher order. We find that the interaction between the Mathieu type of instability and the usual parametric decay instability (we have concentrated here on the decay instability but similar results hold also for the OTSI) is strongest when the condition for the decay instability ($\omega_1 \simeq \omega_k + \Omega_k$ or $\nu_1 \simeq 1$) and the condition for the Mathieu instability ($\Delta \simeq 2\Omega_k$ or $\nu \simeq 2$), are simultaneously satisfied, i.e., when $\nu_1 \simeq -\nu_2 \simeq 1$. The interaction may be either constructive or destructive. Constructive interference is exemplified by the fact that even if both pump amplitudes E_1 and E_2 are below the threshold E_s for the single pump decay instability (in fact, even if $E_1^2 + E_2^2 < E_s^2$) the Mathieu mechanism can still lead to instability, as illustrated in Fig. 5a, 5b and 5c. The destructive aspect is illustrated by the occurrence of nulls in γ as a function of ν_1 or ν_2, nulls which may occur even when $E_1 > E_s$, as illustrated in Fig. 4 and Fig. 7b, and which may extend over a finite interval of ν_1 or ν_2, as in Fig. 7b. As discussed in Sec. IV, the stabilizing or destabilizing effect of the second pump does not vary monotonically

with E_2, as illustrated in Fig. 6 for E_1 below the single pump threshold: the growth rate initially increases with E_2, reaches a maximum and then decreases, eventually vanishing for sufficiently large E_2. If, as is sometimes the case, one wishes to eliminate parametric instabilities, it appears that multiple pumps could be used if their parameters are appropriately chosen. Note that the suppression of the instability observed here occurs with coherent (fixed phase) pumps and hence differs from the use of broadband, randomly phased pumps[8].

It is also important to note the strong dependence of the growth rate on the parameters. For example Figs. 7a and 9c correspond to the same value of the parameters except for a slight difference in the value of ν_1. It is observed that in Fig. 7a the immediate neighborhood of $\nu_2 = -1$ corresponds to region I of Fig. 2 (i.e., only one complex root with $\gamma > 0$), followed by region III after a brief transition to region 2 as $|\delta_2|$ increases, whereas the loop in γ around $\nu_2 = -1$ seen in Fig. 9c corresponds to region II followed by region III as $|\delta_2|$ increases.

The solutions of the dispersion equation discussed in section IV were obtained by solving the infinite determinant using Hill's method. However, in the parameter regime where interesting effects appear, an excellent approximation is obtained by using a 2×2 truncation of that determinant.

Direct solution of the problem in the time domain is used to corroborate the frequency domain results and shows the modulational effects associated with multiple roots of the dispersion equation. Moreover, the Fourier transform of the time domain solutions indicates the spectral line shapes to be expected for the ion and electron densities, at low and high frequencies, respectively. So far as the spectral lines are concerned, the lar-

gest effect of the second pump is to diminish their maximum amplitudes as we approach the nulls of γ, but it also results in some fine structure, e.g. splitting of the lines, appearance of satellites, etc.

A direct extension of this work would include damping effects (collisional or Landau). Inclusion of a phenomenological damping term (damping rate Γ_e) in the fluid equations for the electrons simply replaces ω by $(\omega + i\Gamma_e)$ so Hill's method of solving the infinite determinantal dispersion equation is still applicable. Preliminary calculations show no qualitative changes, aside from the expected diminution of γ. When Γ_e exceeds the ion acoustic frequency Ω_k, the earlier calculation[1] shows that the threshold with two pumps can be considerably lower than with a single pump and it would be interesting to explore the behavior of the growth rates above threshold in that case. An analysis similar to that carried out here could also be used for any of the many parametric instabilities associated with magnetized plasmas. For applications to ionospheric plasmas, it would be important to include the effects of density gradients; for example, each pump may give rise to its own decay instabilities albeit at different altitudes, and these would interact with the Mathieu type of instabilities examined here. Finally, a nonlinear treatment of two pump excitation would give a more realistic prediction of the actual line shapes.

ACKNOWLEDGMENTS:

This work has been supported by DOE Contract DE-AM03-76SF00010 PA 26, Task VIa, and by the Office of Naval Research.

REFERENCES

1. Arnush, D., Nishikawa, K., Fried, B. D., Kennel, C. F., and Wong, A. Y., Phys. Fluids 16, 2270 (1973).
2. Wong, A. Y., Divergilio, W. F., and Iizuka, K., Phys. Lett., 75A, 144 (1979).
3. Minorsky, N., Nonlinear Oscillations (Robert E. Krieger Publishing Company, New York, 1974).
4. Morse, P. M., and Feshback, H., Methods of Theoretical Physics, Vol. 1 (McGraw Hill Book Company Inc., 1953).
5. Fejer, J. A., Cragin, B. L., and Showen, R. L., J. Plasma Phys., 19, 355 (1978).
6. Cheney, W., and Kincaid, D., Numerical Mathematics and Computing (Brooks/Cole Publishing Company, 1980).
7. Bendat, J. S., and Piersol, A. G., Random Data: Analysis and Measurement Procedures (Wiley-Interscience, 1971)
8. Obenschain, S. P., Luhmann, N. C., and Greiling, P. T., Phys. Rev. Lett. 36, 1309 (1976)

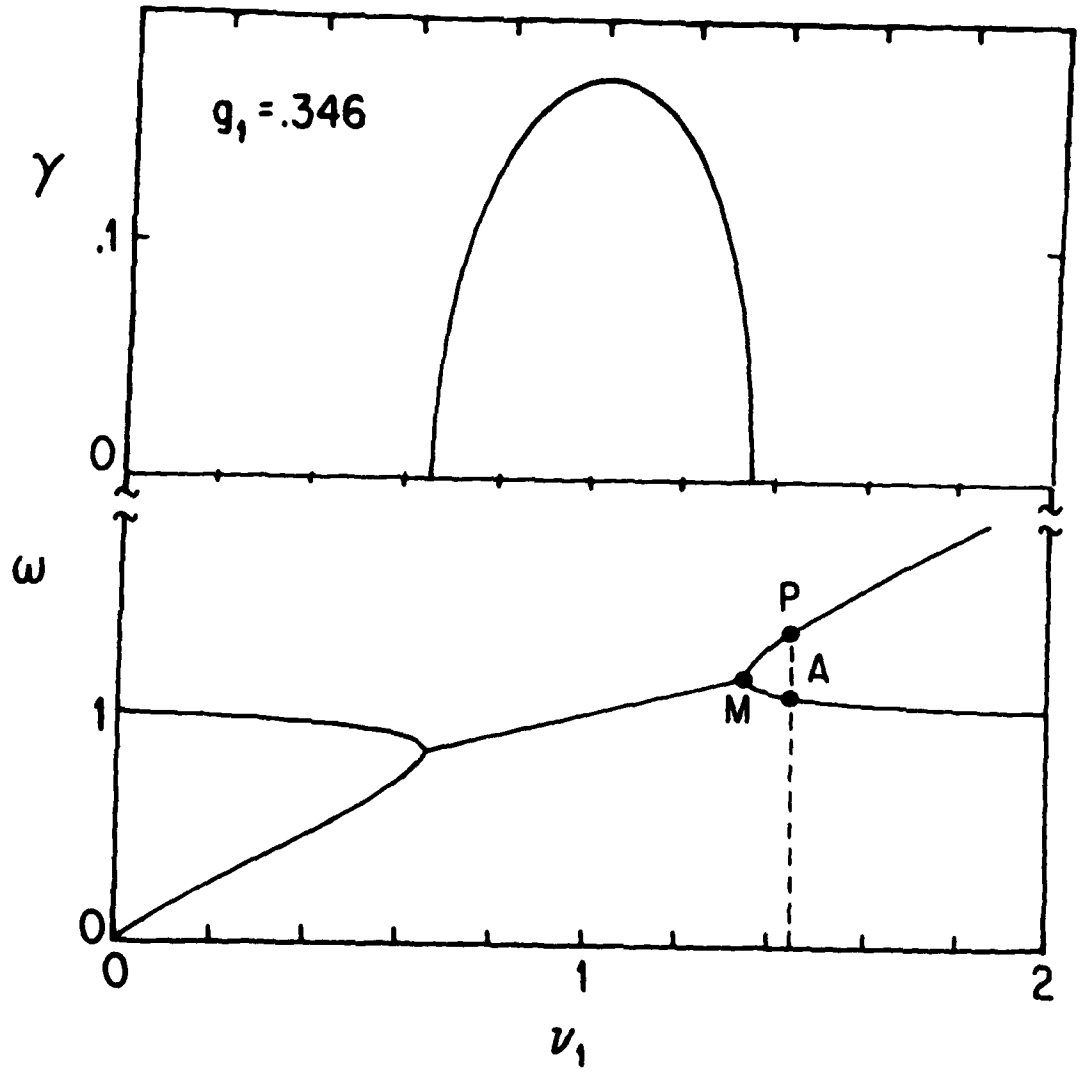

Fig. 1: Growth rate γ (upper half) and real frequency ω (lower half) of the ion acoustic and pump idler modes for the single pump excitation. Points P, A, M are to be used in discussion of Fig. 5a.

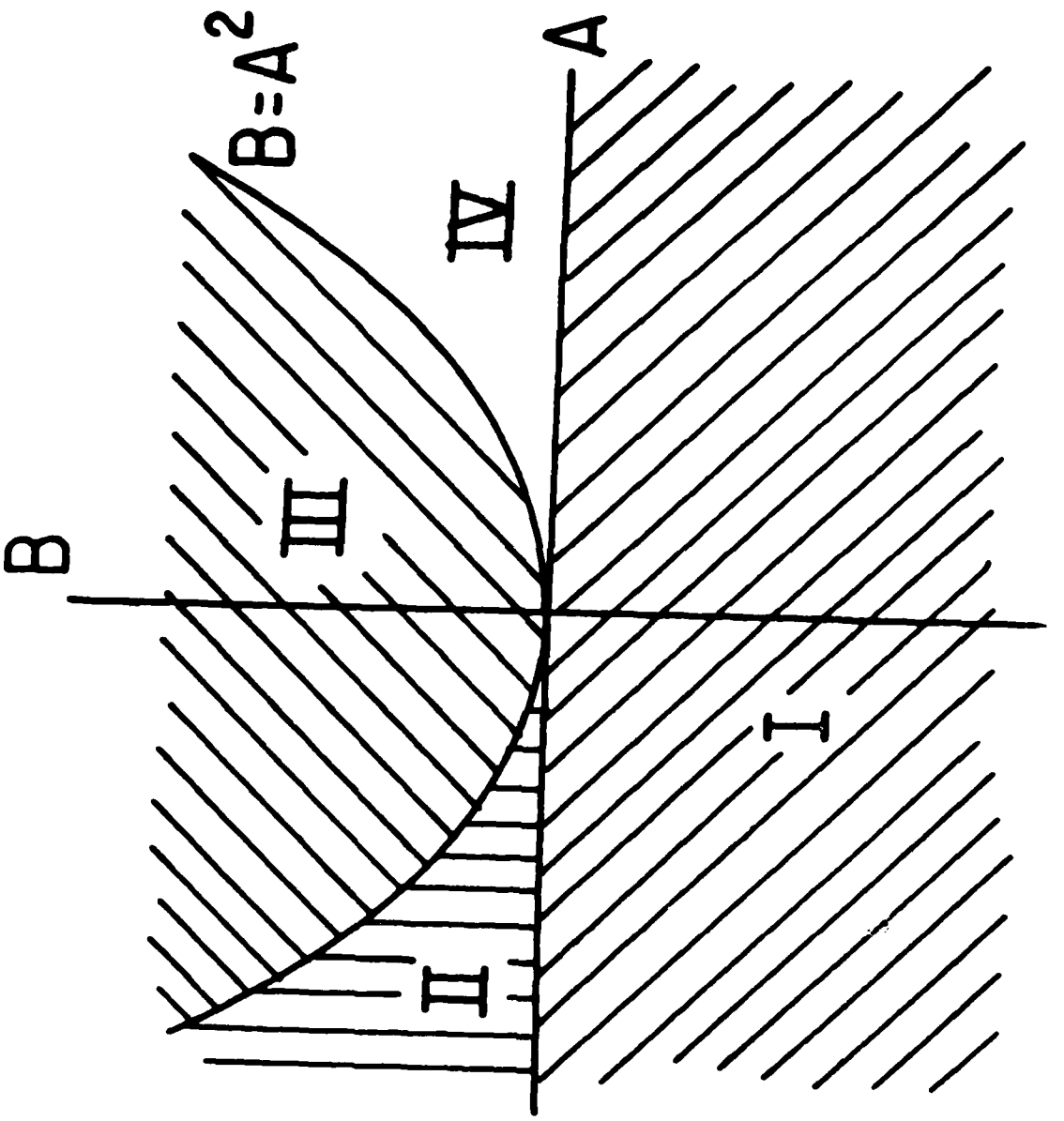

Fig. 2: Stability regions in the plane of the variables A and B defined by (41). The four roots of the biquadratic equation (40) for $y = \omega - \nu$ have the following characteristics in the respective regions of the /2 A-B plane: I) two real roots and two conjugate, purely imaginary roots, II) two pairs of conjugate, purely imaginary roots, III) two pairs of complex conjugate roots, IV) two pairs of equal and opposite real roots.

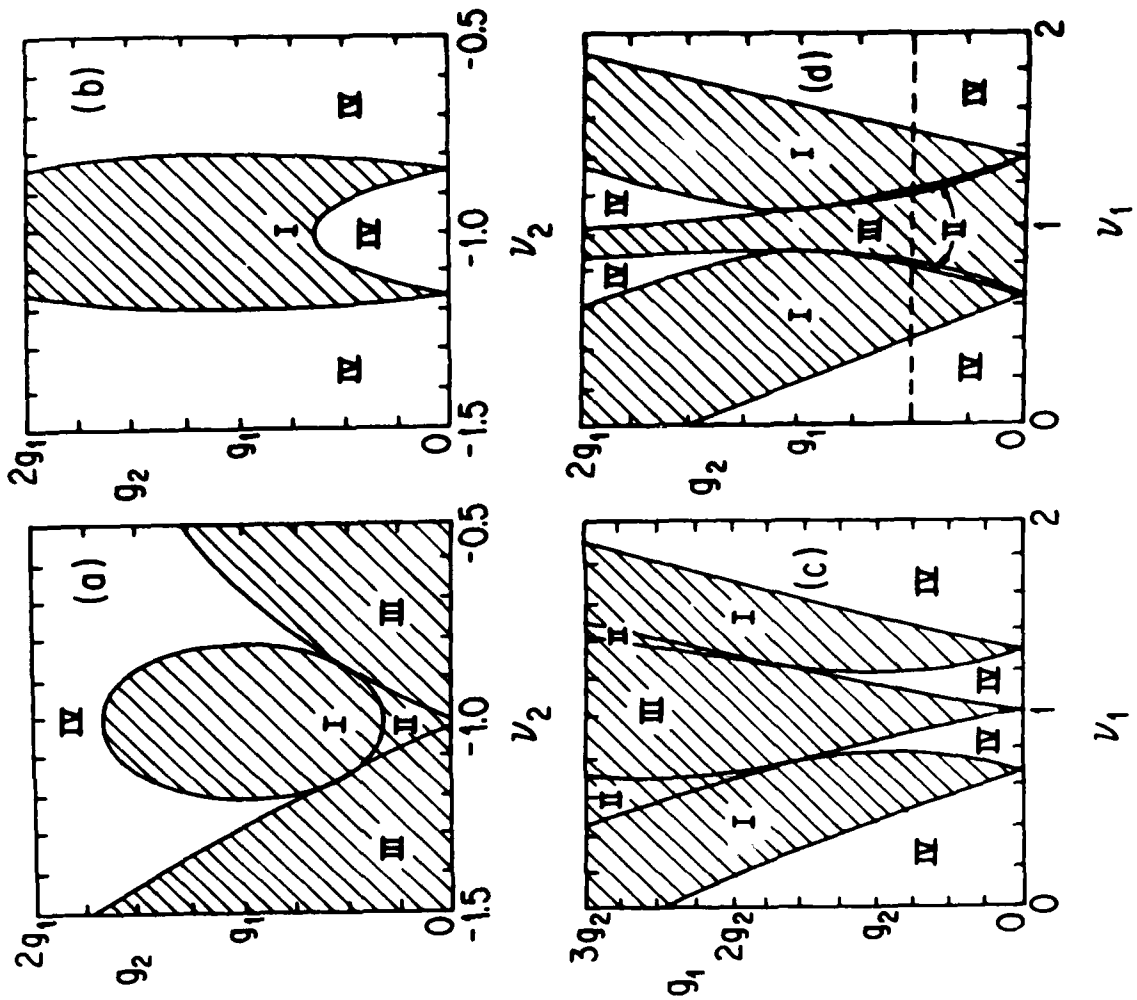

Fig. 3: Stability regions in parameter space as obtained from the approximate solution (42). The shaded regions indicate the unstable zones and the Roman numerals correspond to the labelling in Fig. 2. The dotted line in Fig. 3d is the trajectory in this stability plane corresponding to Fig. 8d. The parameters used are a) $g_1 = .31$, $\nu_1 = 1.2$; b) $g_1 = .125$, $\nu_1 = 1.2$; c) $g_2 = .25$, $\nu_2 = -1.2$; d) $g_1 = .346$, $\nu_2 = -1.1$.

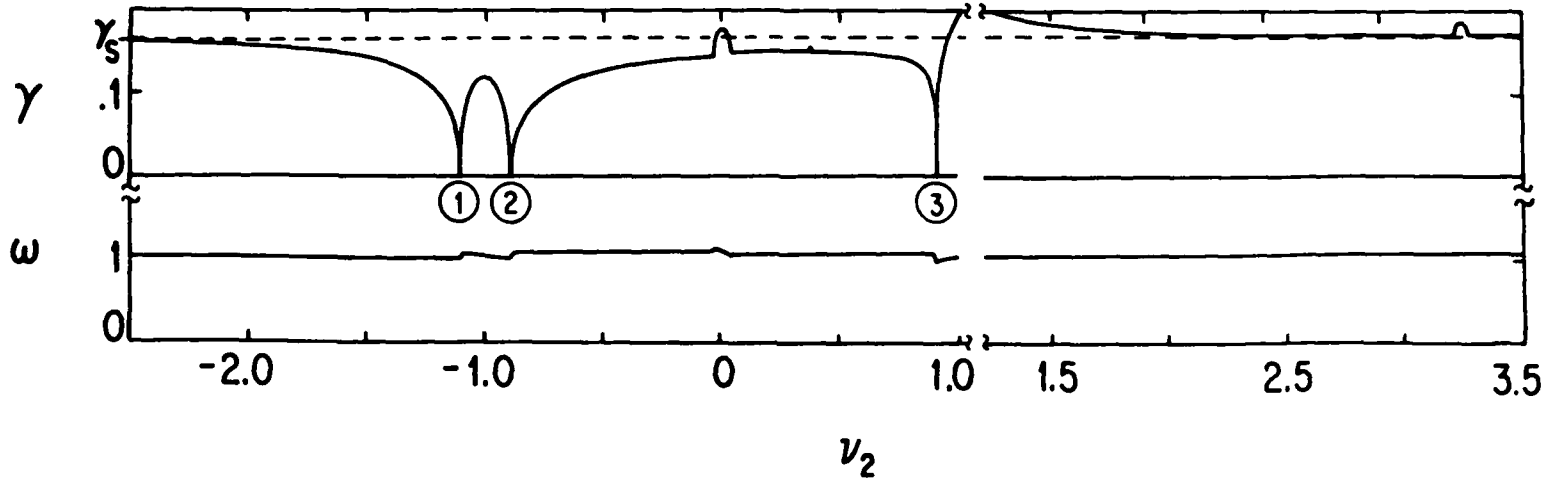

Fig. 4: Growth rate γ (upper half) and frequency ω (lower half) of the ion acoustic mode, normalized to Ω_k, as a function of ν_2 for equal pump amplitudes $g_1 = g_2 = .346$ with $\nu_1 = 1.1$. The zeros of the growth rate, marked as (1), (2) and (3), correspond to $\nu_2 = -\nu_1$, $\nu_1 - \nu_2 = 2$ and $\nu_1 + \nu_2 = 2$ respectively. The broken line at $\gamma = \gamma_s$ corresponds to the single pump growth rate for $\nu_1 = 1.1$ and $g_1 = .346$.

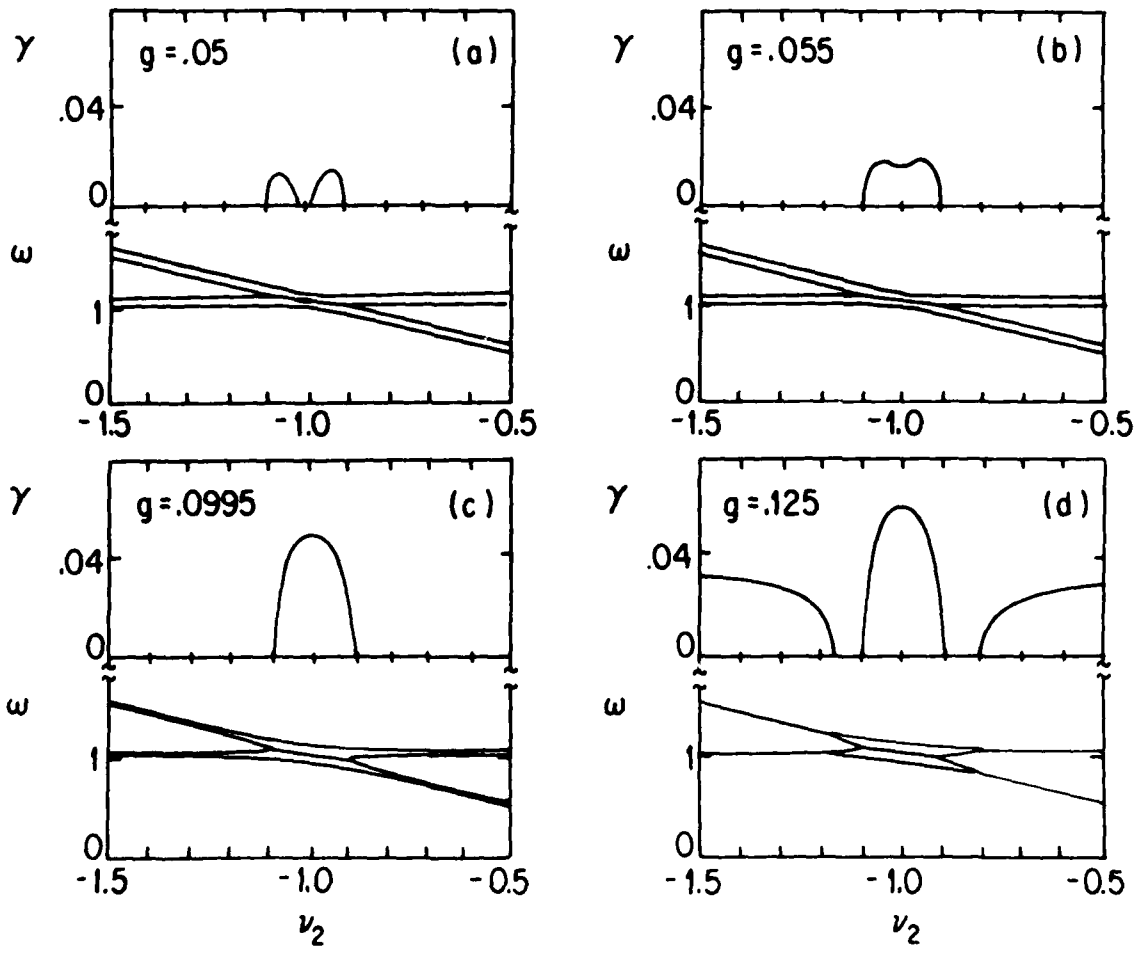

Fig. 5: Growth rate γ (upper half) and frequency ω (lower half) of the ion acoustic and pump idler modes in the double resonance region for equal pump amplitudes $g_1 = g_2 = g$ with $\nu_1 = 1.1$. In Figs. 5(a), 5(b) and 5(c) the pump amplitudes are below the single pump instability threshold $g < g_s$; in Fig. 5(d) $g > g_s$.

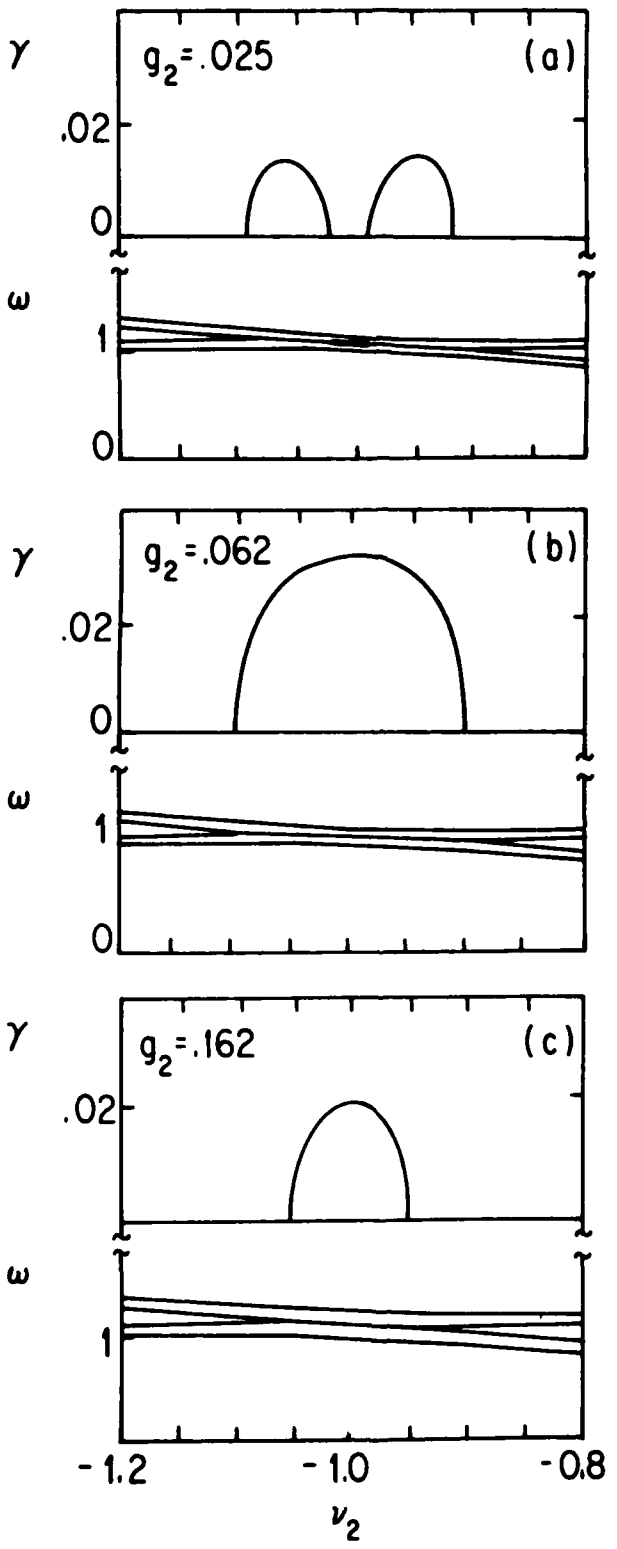

Fig. 6: Growth rate γ (upper half) and frequency ω (lower half) of the ion acoustic and idler pump modes as a function of ν_2 in the double resonance region for unequal pump amplitudes with $\nu_1 = 1.1$ and $g_1 = .075 < g_s \simeq .095$.

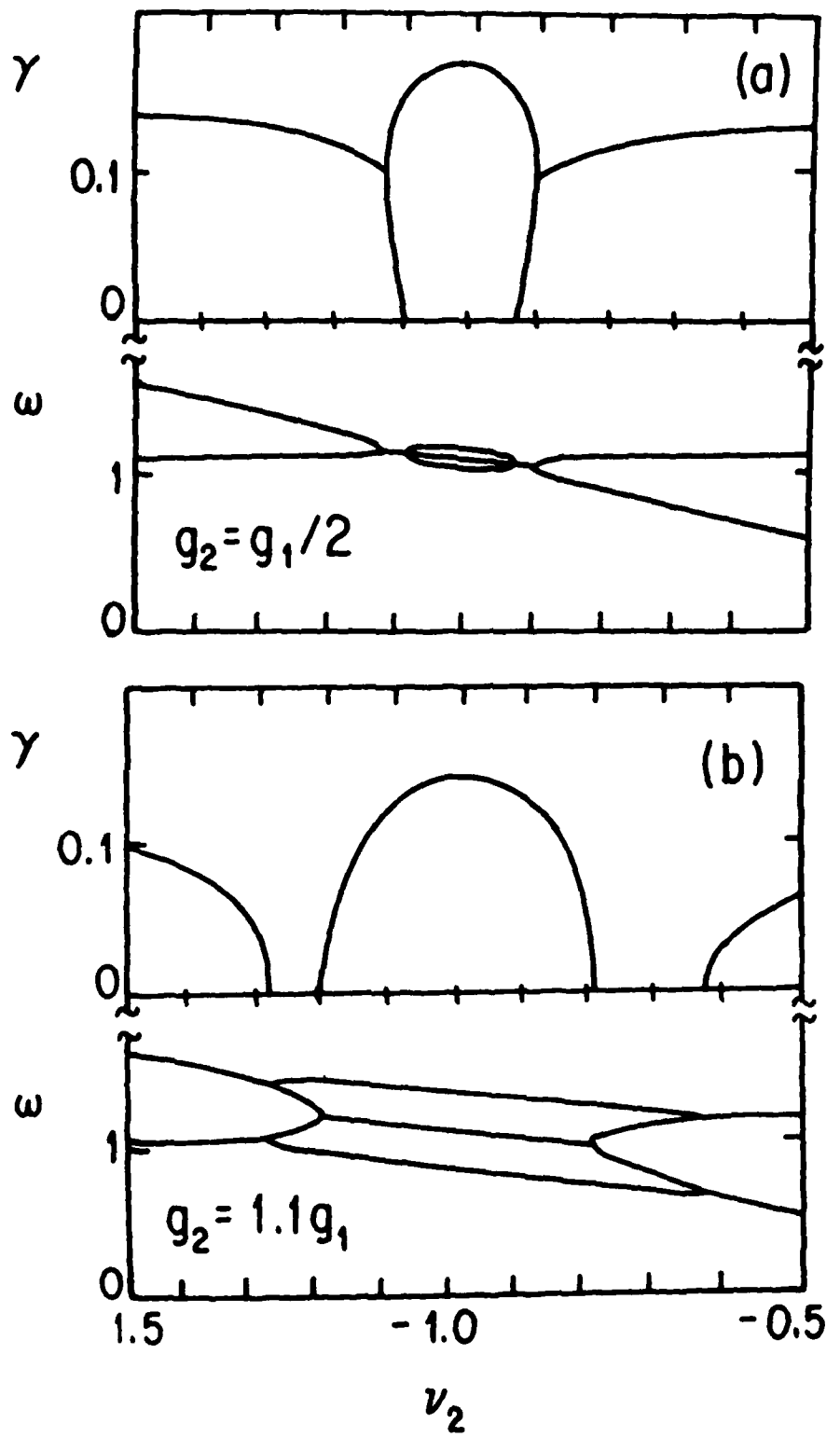

Fig. 7: Growth rate γ (upper half) and frequency ω (lower half) of the ion acoustic and pump modes as a function of ν_2 in the double resonance region for unequal pump amplitudes with $\nu_1 = 1.2$ and $g_1 = .346 > g_s \simeq .18$.

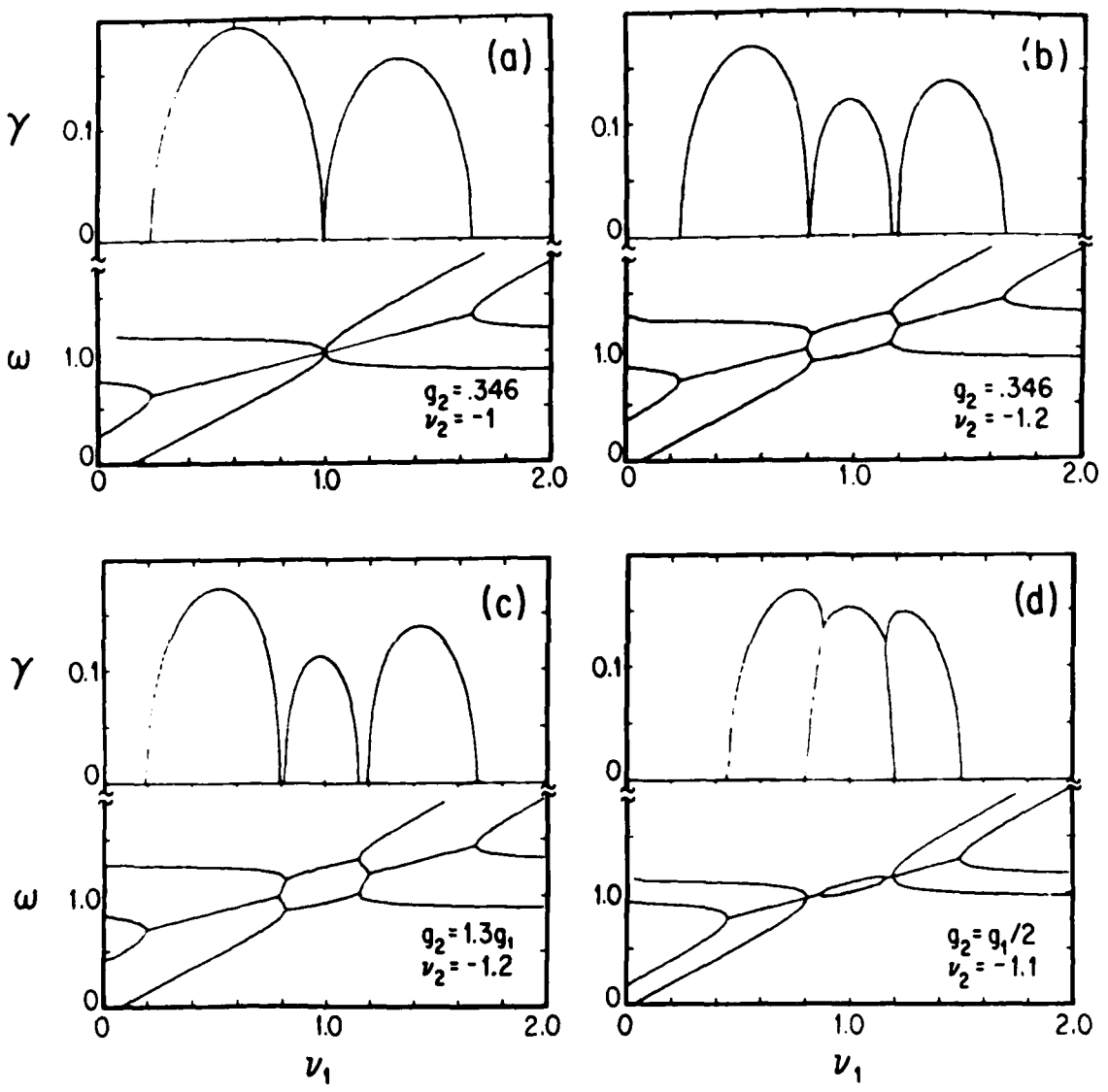

Fig. 8: Growth rate γ (upper half) and frequencies ω (lower half) of the ion acoustic and pump modes as a function of ν_1 with $g_1 = .346$ and and various values of g_2, ν_2 as noted.

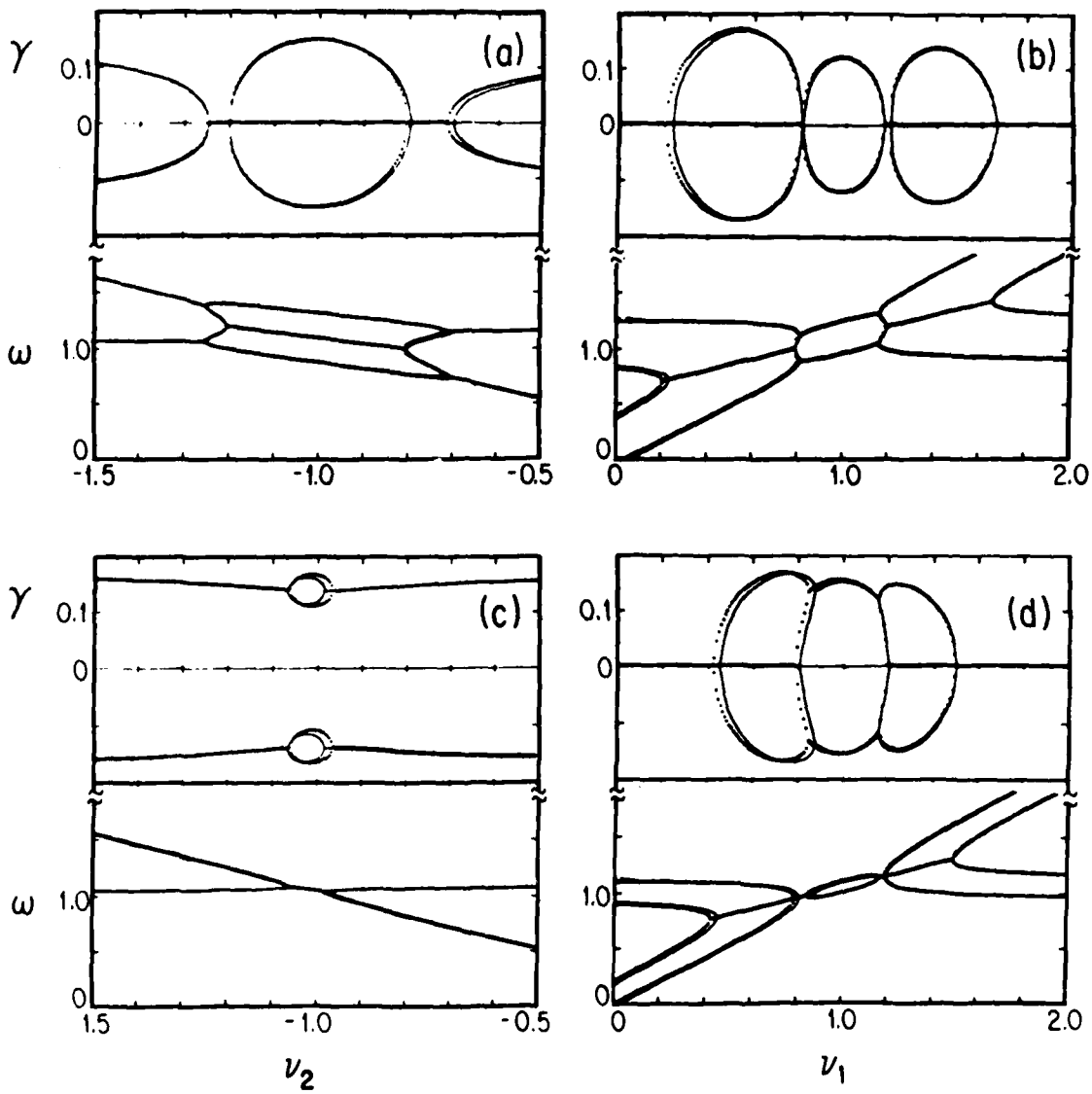

Fig. 9: Comparison of the four solutions of the exact dispersion relation (34) (solid) and the approximation (42) (dotted) for various choices of parameters in the double resonance region. The parameters are (a) $g_1 = g_2 = .346$, $\nu_1 = 1.2$; (b) $g_1 = g_2 = .346$, $\nu_2 = -1.2$; (c) $g_1 = .346$, $g_2 = g_1/2$, $\nu_1 = 1.1$; (d) $g_2 = g_1/2$, $\nu_2 = -1.1$.

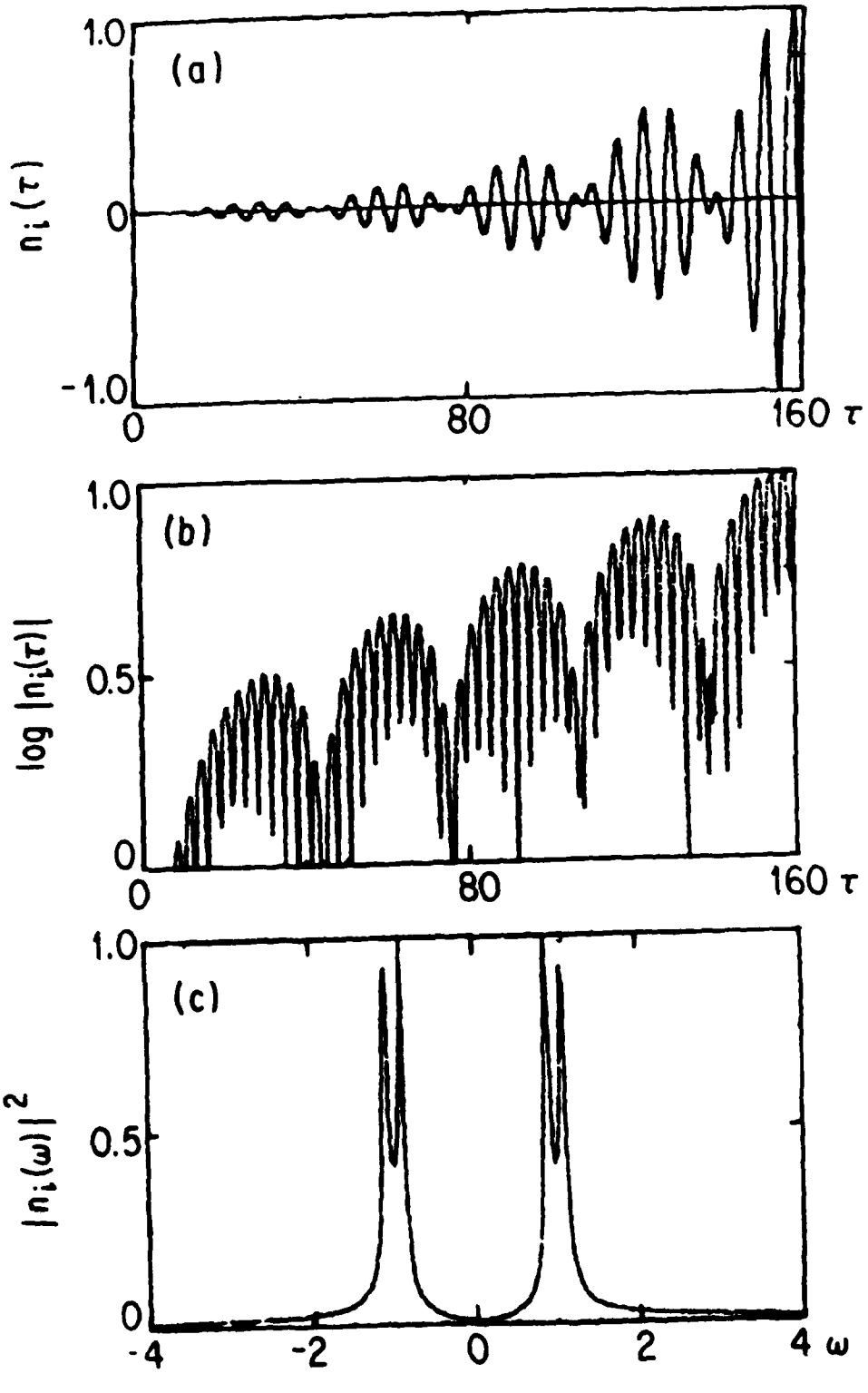

Fig. 10: Time and frequency dependence of the ion density n_i. (a) Ion density $n_i(t)$ for $g_1 = g_2 = .346$, $\nu_1 = 1.1$, $\nu_2 = -0.88$; (b) $\text{Log}|n_i(t)|$ as a function of time for $g_1 = g_2 = .346$, $\nu_1 = 1.1$, $\nu_2 = -0.88$; (c) Power spectrum $|n_i(\omega)|^2$ corresponding to Fig. 10(a).

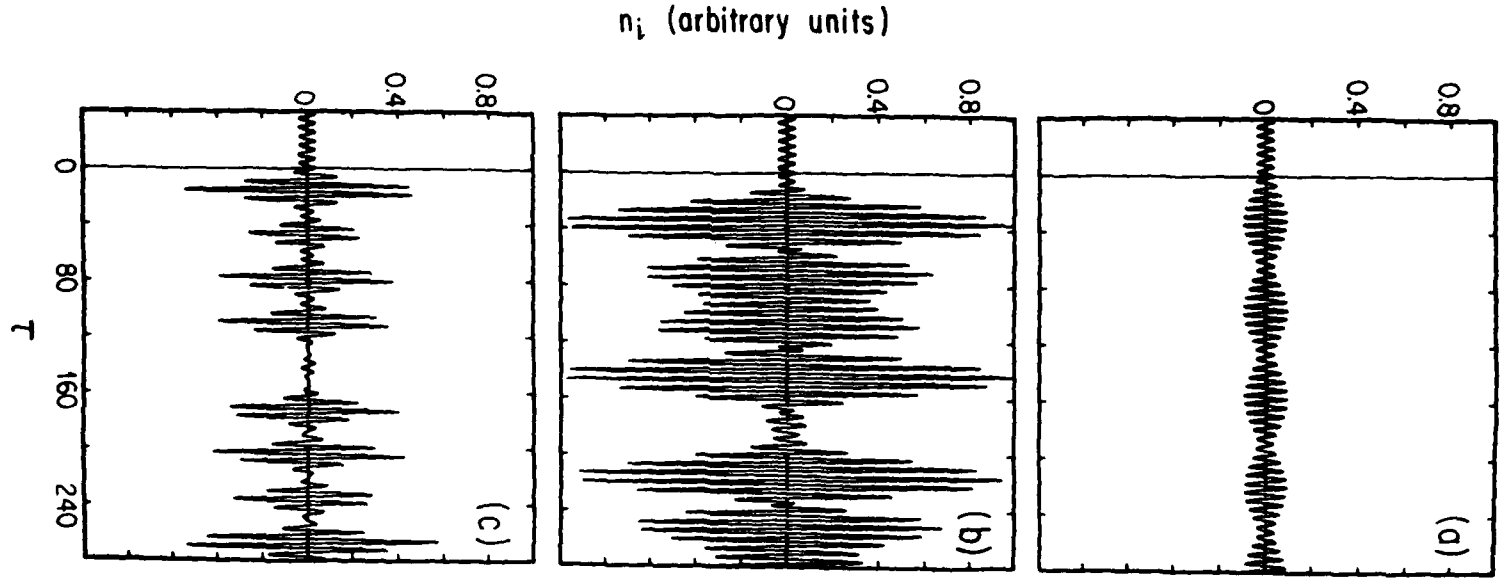

Fig. 11: Ion density $n_i(t)$ for parameters corresponding to the nulls of Fig. 4 with $g_1 = g_2 = .346$, $\nu_1 = 1.1$.
(a) corresponds to null 1 in Fig. 4 ($\nu_2 = -\nu_1$); (b) corresponds to null 2 in Fig. 4 ($\nu_1 - \nu_2 = 2$); (c) corresponds to null 3 in Fig. 4 ($\nu_1 + \nu_2 = 2$).

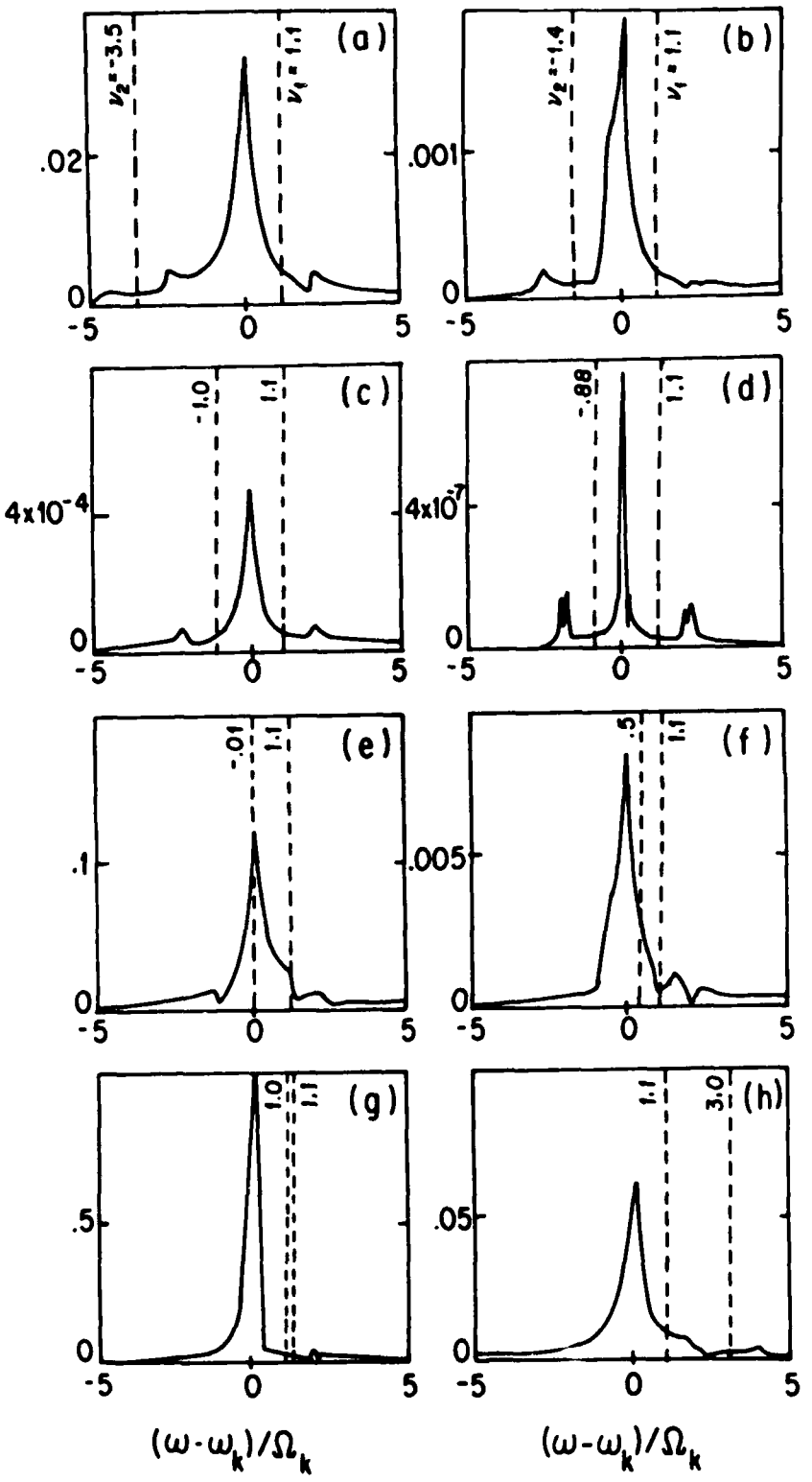

Fig. 12: Electron density spectrum $|n_e(\omega)|^2$ for $g_1 = g_2 = .346$, $\nu_1 = 1.1$ plotted as a function of $(\omega - \omega_k)/\Omega_k$ for various choices of ν_2. The values of $(\omega - \omega_k)/\Omega_k$ corresponding to the two pumps are indicated by the dotted lines.

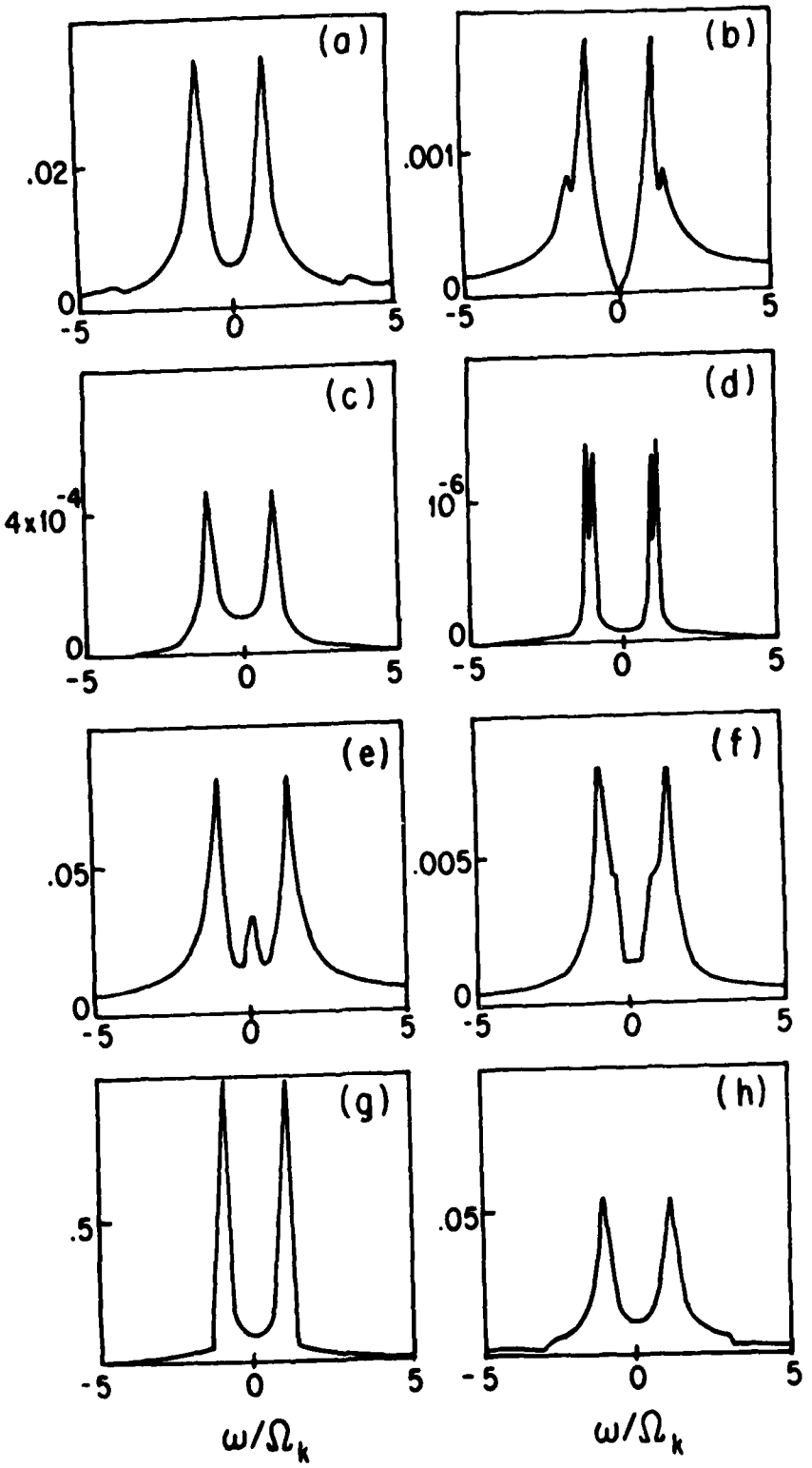

Fig. 13: Ion density spectrum $|n_i(\omega)|^2$ for the same parameters as in Fig. 12.

PPG-734 "Containment of Laser Produced High Beta Plasmas by Relatively Weak Surface Magnetic Fields," A. Y. Wong, (August, 1983), submitted to Physical Review Letters.

PPG-735 "Thomson Scattering Measurements of Electron Power Losses in the UCLA Didecapole SURMAC," K. Jones, Ph.D. Dissertation, August 1983.

PPG-736 "Bounded, Electrostatic Particle Simulation Code on the UCLA CHI Computer System," V. K. Decyk.

PPG-737 "Magnetic Field Line Reconnection Experiments, Part 6 - Magnetic Turbulence", W. Gekelman & R. L. Stenzel, submitted to Jour. Geophys. Res., August 1983

PPG-738 "Accretion Disk Electrodynamics", F. V. Coroniti, August, 1983 for International Astronomical Union Symposium/ Highlights of Astronomy

PPG-739 "Neutron Radiation Effects on the Structure of the Particle Beam Fusion Target Development Facility," N. Ghoniem, not for publication, (August, 1983).

PPG-740 "Ion Trapping Saturation of the Brillouin Instability ", C. E. Clayton, C. Joshi, F. F. Chen, submitted to PHys. Rev. Lett., August 1983.

PPG-741 "Laboratory Experiments on Current Sheet Disruptions, Double Layers, Turbulence and Reconnection," by R. L. Stenzel, AGU Meeting, August, 1983.

PPG-742 "An Advanced Pump Limiter Experiment of Large Toroidal Extent--ALT 2," Bob Conn, et al., not for publication, August 1983.

PPG-743 "Constitutive Design Equations for Creep Deformation of HT-9," Robert Amodeo & Nasr Ghoniem, submitted to Journal of Nuclear Material, August, 1983.

PPG-744 "The Interaction of High Energy Collision Cascades with Helium Field Cavities and Carbide Precipitations," Philip Chou & Nasr Ghoniem, submitted to Journal of Nuclear Material, August, 1983.

PPG-745 "Behavior of the Ponderomotive Effect Near Gyroresonance", B. M. Lamb, G. Dimonte and G. J. Morales, submitted to Physics of Fluids, September 1983

PPG-746 "Collisional and Convective Thresholds for Ramen Backscatter", B. Amini, F. F. Chen, not for pub., September 1983.

PPG-747 "Observations of Lower Hybrid Noise in the Io Plasma Torus and Anomalous Plasma Heating Rates," D. D. Barbosa, F. V. Coroniti, W. S. Kurth & F. L. Scarf, Sept. 1983.

PPG-748 "Ohmic Heating of the Polar F-Region by HF Pulses," M. M. Shoucri & G. J. Morales, J. E. Maggs, submitted to JGR, October 1983.

PPG-749 "Voyager I: Evidence for Ion Cyclotron Instability in the Vicinity of the Io Plasma Torus," R. Thorne and F. Scarf, October, 1983.

PPG-750 "An Energy Principle for High-Latitude Electrodynamics," D. D. Barbosa, to be submitted to JGR, October, 1983.

PPG-751 "Relativistic Dispersion and the Generation of Auroral Kilometric Radiation," P. L. Pritchett, to be submitted to Geo. Res. Letts., October 1983.

PPG-752 "Laser Diagnostics of Magnetically Confined Thermonuclear Plasmas," N. C. Luhmann & W. A. Peebles, (October, 1983).

PPG-753 "Panel Report on Low Activation Materials for Fusion Applications Report to DOE Final Draft, June, 1983," R. W. Conn, October 1983.

PPG-754 "Kinetic Effects and Stabilization of Flute Instability in Sheared Magnetic Fields," K. Nakamura, Ph.D. Dissertation, November, 1983.

PPG-755 "Nonlinear Efficiency and Bandwidth Of A Slow Wave Cyclotron Amplifier," A. T. Lin, W. W. Chang and K. R. Chu, November 1983.

PPG-756 "Triggered Tearing Modes in a Magnetic Neutral Sheet," R. Stenzel & W. Gekelman, submitted to Journal of Geophysical Review, November 1983.

PPG-757 "Initial Start-Up of a Tandem Mirror Reactor," M. A. Firestone, T. K. Mau & R. W. Conn, to be presented at the 10th Symposium on Fusion Engineering, Philadelphia, December, 1983.

PPG-758 "Plasma Heating and Acceleration by Strong Magnetosonic Waves Propagating Obliquely to a Magnetostatic Field," B. Lembege and J.M. Dawson, December 1983.

PPG-759 "The Physics of the Ion Acoustic Wave Driven by the Stimulated Brillouin Scattering Instability," C. E. Clayton, December 1983.

PPG-760 "Three Dimensional Self-Collapse of Langmuir Waves," A. Y. Wong & P. Y. Cheung, to be submitted to Physical Review Letters, December 1983.

PPG-761 "Ion Skin Depth Scaling and Cusp Distortion in Picket Fence Geometry," S.T. Ratliff and J.M. Dawson, December,1983.

PPG-762 "A Parametric Study of the First Critical Mach Number for a Fast MHD Shock," J. P. Edmiston & C. F. Kennel, to be submitted to Journal of Plasma Physics, December, 1983.

PPG-763 "Growth Rates of Parametric Instabilities Driven By Two Pumps," J. Milovich, B. D. Fried, G. J. Morales, January (1984).


8
TIC